

Adversarial Examples can be Effective Data Augmentation for Unsupervised Machine Learning

Chia-Yi Hsu¹, Pin-Yu Chen², Songtao Lu², Sijia Liu³, Chia-Mu Yu¹

¹National Yang Ming Chiao Tung University

²IBM Research

³Michigan State University

{chiayihsu8315, chiamuyu}@gmail.com, {pin-yu.chen, songtao}@ibm.com, liusiji5@msu.edu

Abstract

Adversarial examples causing evasive predictions are widely used to evaluate and improve the robustness of machine learning models. However, current studies focus on supervised learning tasks, relying on the ground-truth data label, a targeted objective, or supervision from a trained classifier. In this paper, we propose a framework of generating adversarial examples for **unsupervised** models and demonstrate novel applications to data augmentation. Our framework exploits a mutual information neural estimator as an information-theoretic similarity measure to generate adversarial examples without supervision. We propose a new MinMax algorithm with provable convergence guarantees for efficient generation of unsupervised adversarial examples. Our framework can also be extended to supervised adversarial examples. When using unsupervised adversarial examples as a simple plug-in data augmentation tool for model retraining, significant improvements are consistently observed across different unsupervised tasks and datasets, including data reconstruction, representation learning, and contrastive learning. Our results show novel methods and considerable advantages in studying and improving unsupervised machine learning via adversarial examples.

1 Introduction

Adversarial examples are known as prediction-evasive attacks on state-of-the-art machine learning models (e.g., deep neural networks), which are often generated by manipulating native data samples while maintaining high similarity measured by task-specific metrics such as L_p -norm bounded perturbations (Goodfellow, Shlens, and Szegedy 2015; Biggio and Roli 2018). Due to the implications and consequences on mission-critical and security-centric machine learning tasks, adversarial examples are widely used for robustness evaluation of a trained model and for robustness enhancement during training (i.e., adversarial training).

Despite of a plethora of adversarial attacking algorithms, the design principle of existing methods is primarily for *supervised* learning models — requiring either the true label or a targeted objective (e.g., a specific class label or a reference sample). Some recent works have extended to the *semi-supervised* setting, by leveraging supervision from a classifier (trained on labeled data) and using the predicted

(I) Mathematical notation

$M^{\text{sup}}/M^{\text{unsup}}$: trained supervised/unsupervised machine learning models

x/x_{adv} : original/adversarial data sample

$\ell_x^{\text{sup}}/\ell_x^{\text{unsup}}$: supervised/unsupervised loss function in reference to x

(II) *Supervised tasks*
(e.g. classification)

(III) *Unsupervised tasks* (our proposal)
(e.g. data reconstruction, contrastive learning)

x_{adv} is **similar** to x but
 $M^{\text{sup}}(x_{\text{adv}}) \neq M^{\text{sup}}(x)$

x_{adv} is **dissimilar** to x but
 $\ell_x^{\text{unsup}}(x_{\text{adv}}|M^{\text{unsup}}) \leq \ell_x^{\text{unsup}}(x|M^{\text{unsup}})$

Table 1: Illustration of adversarial examples for supervised/unsupervised machine learning tasks. Both settings use a native data sample x as reference. For supervised setting, adversarial examples refer to *similar* samples of x causing inconsistent predictions. For unsupervised setting, adversarial examples refer to *dissimilar* samples yielding smaller loss than x , relating to generalization errors on low-loss samples.

labels on unlabeled data for generating (semi-supervised) adversarial examples (Miyato et al. 2018; Zhang et al. 2019; Stanforth et al. 2019; Carmon et al. 2019). On the other hand, recent advances in unsupervised and few-shot machine learning techniques show that task-invariant representations can be learned and contribute to downstream tasks with limited or even without supervision (Ranzato et al. 2007; Zhu and Goldberg 2009; Zhai et al. 2019), which motivates this study regarding their robustness. Our goal is to provide efficient robustness evaluation and data augmentation techniques for unsupervised (and self-supervised) machine learning models through *unsupervised* adversarial examples (UAEs). Table 1 summarizes the fundamental difference between conventional supervised adversarial examples and our UAEs. Notably, our UAE generation is supervision-free because it solely uses an information-theoretic similarity measure and the associated unsupervised learning objective function. It does not use any supervision such as label information or prediction from other supervised models.

In this paper, we aim to formalize the notion of UAE, establish an efficient framework for UAE generation, and demonstrate the advantage of UAEs for improving a variety of unsupervised machine learning tasks. We summarize our main contributions as follows.

- We propose a new per-sample based mutual information neural estimator (MINE) between a pair of original and modified data samples as an information-theoretic similarity measure and a supervision-free approach for generating UAE. For

instance, see UAEs for data reconstruction in Figure 5 of supplementary material. While our primary interest is generating adversarial examples for unsupervised learning models, we also demonstrate that our per-sample MINE can be used to generate adversarial examples for supervised learning models with improved visual quality.

- We formulate the generation of adversarial examples with MINE as a constrained optimization problem, which applies to both supervised and unsupervised machine learning tasks. We then develop an efficient MinMax optimization algorithm (Algorithm 1) and prove its convergence. We also demonstrate the advantage of our MinMax algorithm over the conventional penalty-based method.
- We show a novel application of UAEs as a simple plug-in data augmentation tool for several unsupervised machine learning tasks, including data reconstruction, representation learning, and contrastive learning on image and tabular datasets. Our extensive experimental results show outstanding performance gains (up to 73.5% performance improvement) by retraining the model with UAEs.

2 Related Work and Background

2.1 Adversarial Attack and Defense

For supervised adversarial examples, the attack success criterion can be either *untargeted* (i.e. model prediction differs from the true label of the corresponding native data sample) or *targeted* (i.e. model prediction targeting a particular label or a reference sample). In addition, a similarity metric such as L_p -norm bounded perturbation is often used when generating adversarial examples. The projected gradient descent (PGD) attack (Madry et al. 2018) is a widely used approach to find L_p -norm bounded supervised adversarial examples. Depending on the attack threat model, the attacks can be divided into white-box (Szegedy et al. 2013; Carlini and Wagner 2017b), black-box (Chen et al. 2017; Brendel, Rauber, and Bethge 2018; Liu et al. 2020), and transfer-based (Nitin Bhagoji et al. 2018; Papernot et al. 2017) approaches.

Although a plethora of defenses were proposed, many of them failed to withstand advanced attacks (Carlini and Wagner 2017a; Athalye, Carlini, and Wagner 2018). Adversarial training (Madry et al. 2018) and its variants aiming to generate worst-case adversarial examples during training are so far the most effective defenses. However, adversarial training on supervised adversarial examples can suffer from undesirable tradeoff between robustness and accuracy (Su et al. 2018; Tsipras et al. 2019). Following the formulation of untargeted supervised attacks, recent studies such as (Cemgil et al. 2020) generate adversarial examples for unsupervised tasks by finding an adversarial example within an L_p -norm perturbation constraint that maximizes the training loss. In contrast, our approach aims to find adversarial examples that have low training loss but are dissimilar to the native data (see Table 1), which plays a similar role to the category of “on-manifold” adversarial examples governing generalization errors (Stutz, Hein, and Schiele 2019). In supervised setting, (Stutz, Hein, and Schiele 2019) showed that adversarial training with L_p -norm constrained perturbations may find off-manifold adversarial examples and hurt generalization.

2.2 Mutual Information Neural Estimator

Mutual information (MI) measures the mutual dependence between two random variables X and Z , defined as $I(X, Z) = H(X) - H(X|Z)$, where $H(X)$ denotes the (Shannon) entropy of X and $H(X|Z)$ denotes the conditional entropy of X given Z . Computing MI can be difficult without knowing the marginal and joint probability distributions (\mathbb{P}_X , \mathbb{P}_Z , and \mathbb{P}_{XZ}). For efficient computation, the mutual information neural estimator (MINE) with consistency guarantees is proposed in (Belghazi et al. 2018). Specifically, MINE aims to maximize the lower bound of the exact MI using a model parameterized by a neural network θ , defined as $I_\Theta(X, Z) \leq I(X, Z)$, where Θ is the space of feasible parameters of a neural network, and $I_\Theta(X, Z)$ is the neural information quantity defined as $I_\Theta(X, Z) = \sup_{\theta \in \Theta} \mathbb{E}_{\mathbb{P}_{XZ}}[T_\theta] - \log(\mathbb{E}_{\mathbb{P}_X \otimes \mathbb{P}_Z}[e^{T_\theta}])$. The function T_θ is parameterized by a neural network θ based on the Donsker-Varadhan representation theorem (Donsker and Varadhan 1983). MINE estimates the expectation of the quantities above by shuffling the samples from the joint distribution along the batch axis or using empirical samples $\{x_i, z_i\}_{i=1}^n$ from \mathbb{P}_{XZ} and $\mathbb{P}_X \otimes \mathbb{P}_Z$ (the product of marginals).

MINE has been successfully applied to improve representation learning (Hjelm et al. 2019; Zhu, Zhang, and Evans 2020) given a dataset. However, for the purpose of generating an adversarial example for a given data sample, the vanilla MINE is not applicable because it only applies to a batch of data samples (so that empirical data distributions can be used for computing MI estimates) but not to single data sample. To bridge this gap, we will propose two MINE-based sampling methods for single data sample in Section 3.1.

3 Methodology

3.1 MINE of Single Data Sample

Given a data sample x and its perturbed sample $x + \delta$, we construct an auxiliary distribution using their random samples or convolution outputs to compute MI via MINE as a similarity measure, which we denote as “per-sample MINE”.

Random Sampling Using compressive sampling (Candès and Wakin 2008), we perform independent Gaussian sampling of a given sample x to obtain a batch of K compressed samples $\{x_k, (x + \delta)_k\}_{k=1}^K$ for computing $I_\Theta(x, x + \delta)$ via MINE. We refer the readers to the supplementary material (SuppMat 6.2, 6.3) for more details. We also note that random sampling is agnostic to the underlying machine learning model since it directly applies to the data sample.

Convolution Layer Output When the underlying neural network model uses a convolution layer to process the input data (which is an almost granted setting for image data), we propose to use the output of the first convolution layer of a data input, denoted by $\text{conv}(\cdot)$, to obtain K feature maps $\{\text{conv}(x)_k, \text{conv}(x + \delta)_k\}_{k=1}^K$ for computing $I_\Theta(x, x + \delta)$. We provide the detailed algorithm for convolution-based per-sample MINE in SuppMat 6.2.

Evaluation We use the CIFAR-10 dataset and the same neural network as in Section 4.2 to provide qualitative and quantitative evaluations on the two per-sample MINE methods for image classification. Figure 1 shows their visual com-

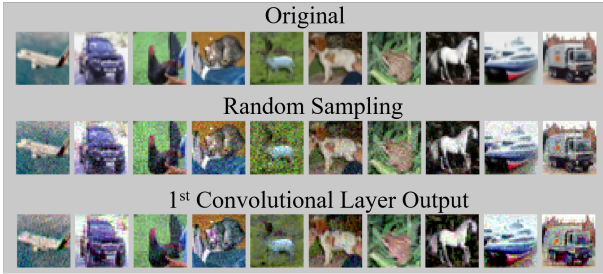


Figure 1: Visual comparison of MINE-based untargeted supervised adversarial examples (with $\epsilon = 1$) on CIFAR-10.

Per-sample MINE Method	FID	KID
Random Sampling (10 runs, $K = 96$)	339.47 ± 8.07	14.86 ± 1.45
1st Convolution Layer Output ($K = 96$)	344.231	10.78

Table 2: Frechet and kernel inception distances (FID/KID) between the untargeted adversarial examples of 1000 test samples and the training data in CIFAR-10.

parisons, with the objective of finding the most similar perturbed sample (measured by MINE with the maximal scaled L_∞ perturbation bound $\epsilon = 1$) leading to misclassification. Both random sampling and convolution-based approaches can generate high-similarity prediction-evasive adversarial examples despite of large L_∞ perturbation.

Table 2 compares the Frechet inception distance (FID) (Heusel et al. 2017) and the kernel inception distance (KID) (Bińkowski et al. 2018) between the generated adversarial examples versus the training data (lower value is better). Both per-sample MINE methods have comparable scores. The convolution-based approach attains lower KID score and is observed to have better visual quality as shown in Figure 1. We also tested the performance using the second convolution layer output but found degraded performance. In this paper we use convolution-based approach whenever applicable and otherwise use random sampling.

3.2 MINE-based Attack Formulation

We formalize the objectives for supervised/unsupervised adversarial examples using per-sample MINE. As summarized in Table 1, the supervised setting aims to find *most similar* examples causing prediction evasion, leading to an MINE *maximization* problem. The unsupervised setting aims to find *least similar* examples but having smaller training loss, leading to an MINE *minimization* problem. Both problems can be solved efficiently using our unified MinMax algorithm.

Supervised Adversarial Example Let (x, y) denote a pair of a data sample x and its ground-truth label y . The objective of supervised adversarial example is to find a perturbation δ to x such that the MI estimate $I_\Theta(x, x + \delta)$ is maximized while the prediction of $x + \delta$ is different from y (or being a targeted class $y' \neq y$), which is formulated as

$$\text{Maximize}_\delta \quad I_\Theta(x, x + \delta)$$

such that $x + \delta \in [0, 1]^d$, $\delta \in [-\epsilon, \epsilon]^d$ and $f_x(x + \delta) \leq 0$.

The constraint $x + \delta \in [0, 1]^d$ ensures $x + \delta$ lies in the (normalized) data space of dimension d , and the constraint $\delta \in [-\epsilon, \epsilon]^d$ corresponds to the typical bounded L_∞ perturbation norm. We include this bounded-norm constraint to make direct comparisons to other norm-bounded attacks. One can ignore this constraint by setting $\epsilon = 1$. Finally, the function $f_x^{\text{sup}}(x + \delta)$ is an attack success evaluation function, where $f_x^{\text{sup}}(x + \delta) \leq 0$ means $x + \delta$ is a prediction-evasive adversarial example. For untargeted attack one can use the attack function f_x^{sup} designed in (Carlini and Wagner 2017b), which is $f_x^{\text{sup}}(x') = \text{logit}(x')_y - \max_{j:j \neq y} \text{logit}(x')_j + \kappa$, where $\text{logit}(x')_j$ is the j -th class output of the logit (pre-softmax) layer of a neural network, and $\kappa \geq 0$ is a tunable gap between the original prediction $\text{logit}(x')_y$ and the top prediction $\max_{j:j \neq y} \text{logit}(x')_j$ of all classes other than y . Similarly, the attack function for targeted attack with a class label $y' \neq y$ is $f_x^{\text{sup}}(x') = \max_{j:j \neq y'} \text{logit}(x')_j - \text{logit}(x')_{y'} + \kappa$.

Unsupervised Adversarial Example Many machine learning tasks such as data reconstruction and unsupervised representation learning do not use data labels, which prevents the use of aforementioned supervised attack functions. Here we use an autoencoder $\Phi(\cdot)$ for data reconstruction to illustrate the unsupervised attack formulation. The design principle can naturally extend to other unsupervised tasks. The autoencoder Φ takes a data sample x as an input and outputs a reconstructed data sample $\Phi(x)$. Different from the rationale of supervised attack, for unsupervised attack we propose to use MINE to find the *least similar* perturbed data sample $x + \delta$ with respect to x while ensuring the reconstruction loss of $\Phi(x + \delta)$ is no greater than $\Phi(x)$ (i.e., the criterion of successful attack for data reconstruction). The unsupervised attack formulation is as follows:

$$\text{Minimize}_\delta \quad I_\Theta(x, x + \delta)$$

such that $x + \delta \in [0, 1]^d$, $\delta \in [-\epsilon, \epsilon]^d$ and $f_x(x + \delta) \leq 0$

The first two constraints regulate the feasible data space and the perturbation range. For the L_2 -norm reconstruction loss, the unsupervised attack function is

$$f_x^{\text{unsup}}(x + \delta) = \|x - \Phi(x + \delta)\|_2 - \|x - \Phi(x)\|_2 + \kappa$$

which means the attack is successful (i.e., $f_x^{\text{unsup}}(x + \delta) \leq 0$) if the reconstruction loss of $x + \delta$ relative to the original sample x is smaller than the native reconstruction loss minus a nonnegative margin κ . That is, $\|x - \Phi(x + \delta)\|_2 \leq \|x - \Phi(x)\|_2 - \kappa$. In other words, our unsupervised attack formulation aims to find that most dissimilar perturbed sample $x + \delta$ to x measured by MINE while having smaller reconstruction loss (in reference to x) than x . Such UAs thus relates to generalization errors on low-loss samples because the model is biased toward these unseen samples.

3.3 MINE-based Attack Algorithm

Here we propose a unified MinMax algorithm for solving the aforementioned supervised and unsupervised attack formulations, and provide its convergence proof in Section 3.4. For simplicity, we will use f_x to denote the attack criterion for f_x^{sup} or f_x^{unsup} . Without loss of generality, we will analyze

the supervised attack objective of maximizing I_Θ with constraints. The analysis also holds for the unsupervised case since minimizing I_Θ is equivalent to maximizing I'_Θ , where $I'_\Theta = -I_\Theta$. We will also discuss a penalty-based algorithm as a comparative method to our proposed approach.

MinMax Algorithm (proposed) We reformulate the attack generation via MINE as the following MinMax optimization problem with simple convex set constraints:

$$\text{Min}_{\delta: x+\delta \in [0,1]^d, \delta \in [-\epsilon, \epsilon]^d} \text{Max}_{c \geq 0} F(\delta, c) \triangleq c \cdot f_x^+(x+\delta) - I_\Theta(x, x+\delta)$$

The outer minimization problem finds the best perturbation δ with data and perturbation feasibility constraints $x + \delta \in [0, 1]^d$ and $\delta \in [-\epsilon, \epsilon]^d$, which are both convex sets with known analytical projection functions. The inner maximization associates a variable $c \geq 0$ with the original attack criterion $f_x(x + \delta) \leq 0$, where c is multiplied to the ReLU activation function of f_x , denoted as $f_x^+(x + \delta) = \text{ReLU}(f_x(x + \delta)) = \max\{f_x(x + \delta), 0\}$. The use of f_x^+ means when the attack criterion is not met (i.e., $f_x(x + \delta) > 0$), the loss term $c \cdot f_x(x + \delta)$ will appear in the objective function F . On the other hand, if the attack criterion is met (i.e., $f_x(x + \delta) \leq 0$), then $c \cdot f_x^+(x + \delta) = 0$ and the objective function F only contains the similarity loss term $-I_\Theta(x, x + \delta)$. Therefore, the design of f_x^+ balances the tradeoff between the two loss terms associated with attack success and MINE-based similarity. We propose to use alternative projected gradient descent between the inner and outer steps to solve the MinMax attack problem, which is summarized in Algorithm 1. The parameters α and β denote the step sizes of the minimization and maximization steps, respectively. The gradient $\nabla f_x^+(x + \delta)$ with respect to δ is set to be 0 when $f_x(x + \delta) \leq 0$. Our MinMax algorithm returns the successful adversarial example $x + \delta^*$ with the best MINE value $I_\Theta^*(x, x + \delta^*)$ over T iterations.

Algorithm 1: MinMax Attack Algorithm

- 1: **Require:** data sample x , attack criterion $f_x(\cdot)$, step sizes α and β , perturbation bound ϵ , # of iterations T
 - 2: Initialize $\delta_0 = 0$, $c_0 = 0$, $\delta^* = \text{null}$, $I_\Theta^* = -\infty$, $t = 1$
 - 3: **for** t in T iterations **do**
 - 4: $\delta_{t+1} = \delta_t - \alpha \cdot (c \cdot \nabla f_x^+(x + \delta_t) - \nabla I_\Theta(x, x + \delta_t))$
 - 5: Project δ_{t+1} to $[-\epsilon, \epsilon]$ via clipping
 - 6: Project $x + \delta_{t+1}$ to $[0, 1]$ via clipping
 - 7: Compute $I_\Theta(x, x + \delta_{t+1})$
 - 8: Perform $c_{t+1} = (1 - \frac{\beta}{t^{1/4}}) \cdot c_t + \beta \cdot f_x^+(x + \delta_{t+1})$
 - 9: Project c_{t+1} to $[0, \infty]$
 - 10: **if** $f_x(x + \delta_{t+1}) \leq 0$ and $I_\Theta(x, x + \delta_{t+1}) > I_\Theta^*$ **then**
 - 11: update $\delta^* = \delta_{t+1}$ and $I_\Theta^* = I_\Theta(x, x + \delta_{t+1})$
 - 12: **Return** δ^* , I_Θ^*
-

Penalty-based Algorithm (baseline) An alternative approach to solving the MINE-based attack formulation is the penalty-based method with the objective:

$$\text{Minimize}_{\delta: x+\delta \in [0,1]^d, \delta \in [-\epsilon, \epsilon]^d} c \cdot f_x^+(x + \delta) - I_\Theta(x, x + \delta)$$

where c is a fixed regularization coefficient instead of an optimization variable. Prior arts such as (Carlini and Wagner

2017b) use a binary search strategy for tuning c and report the best attack results among a set of c values. In contrast, our MinMax attack algorithm dynamically adjusts the c value in the inner maximization stage (step 8 in Algorithm 1). In Section 4.2, we will show that our MinMax algorithm is more efficient in finding MINE-based adversarial examples than the penalty-based algorithm. The details of the binary search process are given in SuppMat 6.5. Both methods have similar computation complexity involving T iterations of gradient and MINE computations.

3.4 Convergence Proof of MinMax Attack

As a theoretical justification of our proposed MinMax attack algorithm (Algorithm 1), we provide a convergence proof with the following assumptions on the considered problem:

- **A.1:** The feasible set Δ for δ is compact, and $f_x^+(x + \delta)$ has (well-defined) gradients and Lipschitz continuity (with respect to δ) with constants L_f and l_f . That is, $|f_x^+(x + \delta) - f_x^+(x + \delta')| \leq l_f \|\delta - \delta'\|$ and $\|\nabla f_x^+(x + \delta)\| \leq L_f \|\delta - \delta'\|$, $\forall \delta, \delta' \in \Delta$. Moreover, $I_\Theta(x, x + \delta)$ also has gradient Lipschitz continuity with constant L_I .

- **A.2:** The per-sample MINE is η -stable over iterations for the same input, $|I_{\Theta_{t+1}}(x, x + \delta_{t+1}) - I_{\Theta_t}(x, x + \delta_{t+1})| \leq \eta$.

A.1 holds in general for neural networks since the numerical gradient of ReLU activation can be efficiently computed and the sensitivity (Lipschitz constant) against the input perturbation can be bounded (Weng et al. 2018). The feasible perturbation set Δ is compact when the data space is bounded. A.2 holds by following the consistent estimation proof of the native MINE in (Belghazi et al. 2018).

To state our main theoretical result, we first define the proximal gradient of the objective function as $\mathcal{L}(\delta, c) := [\delta - P_\Delta[\delta - \nabla_\delta F(\delta, c)], c - P_C[c + \nabla_c F(\delta, c)]]$, where $P_{\mathcal{X}}$ denotes the projection operator on convex set \mathcal{X} , and $\|\mathcal{L}(\delta, c)\|$ is a commonly used measure for stationarity of the obtained solution. In our case, $\Delta = \{\delta : x + \delta \in [0, 1]^d \cap \delta \in [-\epsilon, \epsilon]^d\}$ and $\mathcal{C} = \{c : 0 \leq c \leq \bar{c}\}$, where \bar{c} can be an arbitrary large value. When $\|\mathcal{L}(\delta^*, c^*)\| = 0$, then the point (δ^*, c^*) is referred as a game stationary point of the min-max problem (Razaviyayn et al. 2020). Next, we now present our main theoretical result.

Theorem 1. *Suppose Assumptions A.1 and A.2 hold and the sequence $\{\delta_t, c_t, \forall t \geq 1\}$ is generated by the MinMax attack algorithm. For a given small constant ϵ' and positive constant β , let $T(\epsilon')$ denote the first iteration index such that the following inequality is satisfied: $T(\epsilon') := \min\{t \mid \|\mathcal{L}(\delta_t, c_t)\|^2 \leq \epsilon', t \geq 1\}$. Then, when the step-size and approximation error achieved by Algorithm 1 satisfy $\alpha \sim \eta \sim \sqrt{1/T(\epsilon')}$, there exists some constant C such that $\|\mathcal{L}(\delta_{T(\epsilon')}, c_{T(\epsilon')})\|^2 \leq C/\sqrt{T(\epsilon')}$.*

Proof. Please see the supplemental material (SuppMat 6.8).

Theorem 1 states the rate of convergence of our proposed MinMax attack algorithm when provided with sufficient stability of MINE and proper selection of the step sizes. We also remark that under the assumptions and conditions of step-sizes, this convergence rate is standard in non-convex min-max saddle point problems (Lu et al. 2020).

3.5 Data Augmentation using UAE

With the proposed MinMax attack algorithm and per-sample MINE for similarity evaluation, we can generate MINE-based supervised and unsupervised adversarial examples (UAEs). Section 4 will show novel applications of MINE-based UAEs as a simple plug-in data augmentation tool to boost the model performance of several unsupervised machine learning tasks. We observe significant and consistent performance improvement in data reconstruction (up to 73.5% improvement), representation learning (up to 1.39% increase in accuracy), and contrastive learning (1.58% increase in accuracy). The observed performance gain can be attributed to the fact that our UAEs correspond to “on-manifold” data samples having low training loss but are dissimilar to the training data, causing generalization errors. Therefore, data augmentation and re-training with UAEs can improve generalization (Stutz, Hein, and Schiele 2019).

4 Performance Evaluation

In this section, we conduct extensive experiments on a variety of datasets and neural network models to demonstrate the performance of our proposed MINE-based MinMax adversarial attack algorithm and the utility of its generated UAEs for data augmentation, where a high attack success rate using UAEs suggests rich space for data augmentation to improve model performance. Codes are available at <https://github.com/IBM/UAE>.

4.1 Experiment Setup and Datasets

Datasets We provide a brief summary of the datasets: • **MNIST** consists of grayscale images of hand-written digits. The number of training/test samples are 60K/10K. • **SVHN** is a color image dataset set of house numbers extracted from Google Street View images. The number of training/test samples are 73257/26302. • **Fashion MNIST** contains grayscale images of 10 clothing items. The number of training/test samples are 60K/10K. • **Isolet** consists of preprocessed speech data of people speaking the name of each letter of the English alphabet. The number of training/test samples are 6238/1559. • **Coil-20** contains grayscale images of 20 multi-viewed objects. The number of training/test samples are 1152/288. • **Mice Protein** consists of the expression levels (features) of 77 protein modifications in the nuclear fraction of cortex. The number of training/test samples are 864/216. • **Human Activity Recognition** consists of sensor data collected from a smartphone for various human activities. The number of training/test samples are 4252/1492.

Supervised Adversarial Example Setting Both data samples and their labels are used in the supervised setting. We select 1000 test images classified correctly by the pretrained MNIST and CIFAR-10 deep neural network classifiers used in (Carlini and Wagner 2017b) and set the confidence gap parameter $\kappa = 0$ for the designed attack function f_x^{sup} defined in Section 3.2. The attack success rate (ASR) is the fraction of the final perturbed samples leading to misclassification.

Unsupervised Adversarial Example Setting Only the training data samples are used in the unsupervised setting. Their true labels are used in the post-hoc analysis for evaluating

	MNIST		CIFAR-10	
	ASR	MI	ASR	MI
Penalty-based	100%	28.28	100%	13.69
MinMax	100%	51.29	100%	17.14

Table 3: Comparison between MinMax and penalty-based algorithms on MNIST and CIFAR-10 datasets in terms of attack success rate (ASR) and mutual information (MI) value averaged over 1000 adversarial examples.

the quality of the associated unsupervised learning tasks. All training data are used for generating UAEs individually by setting $\kappa = 0$. A perturbed data sample is considered as a successful attack if its loss (relative to the original sample) is no greater than the original training loss (see Table 1). For data augmentation, if a training sample fails to find a successful attack, we will replicate itself to maintain data balance. The ASR is measured on the training data, whereas the reported model performance is evaluated on the test data. The training performance is provided in SuppMat 6.10.

MinMax Algorithm Parameters We use consistent parameters by setting $\alpha = 0.01$, $\beta = 0.1$, and $T = 40$ as the default values. The vanilla MINE model (Belghazi et al. 2018) is used in our per-sample MINE implementation. The parameter sensitivity analysis is reported in SuppMat 6.13.

Computing Resource All experiments are conducted using an Intel Xeon E5-2620v4 CPU, 125 GB RAM and a NVIDIA TITAN Xp GPU with 12 GB RAM.

Models and Codes We defer the summary of the considered machine learning models to the corresponding sections. Our codes are provided in SuppMat.

4.2 MinMax v.s. Penalty-based Algorithms

We use the same untargeted supervised attack formulation and a total of $T = 9000$ iterations to compare our proposed MinMax algorithm with the penalty-based algorithm using 9 binary search steps on MNIST and CIFAR-10. Table 3 shows that while both methods can achieve 100% ASR, MinMax algorithm attains much higher MI values than penalty-based algorithm. The results show that the MinMax approach is more efficient in finding MINE-based adversarial examples, which can be explained by the dynamic update of the coefficient c in Algorithm 1.

Figure 2 compares the statistics of MI values over attack iterations. One can find that as iteration count increases, MinMax algorithm can continue improving the MI value, whereas penalty-based algorithm saturates at a lower MI value due to the use of fixed coefficient c in the attack process. In the remaining experiments, we will report the results using MinMax algorithm due to its efficiency.

4.3 Qualitative Visual Comparison

Figure 3 presents a visual comparison of MNIST supervised adversarial examples crafted by MinMax attack and the PGD attack with 100 iterations (Madry et al. 2018) given different ϵ values governing the L_∞ perturbation bound. The main difference is that MinMax attack uses MINE as an additional similarity regulation while PGD attack only uses L_∞ norm.

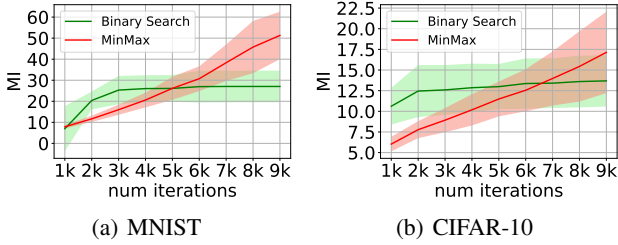


Figure 2: Mean and standard deviation of mutual information (MI) value versus attack iteration over 1000 samples.

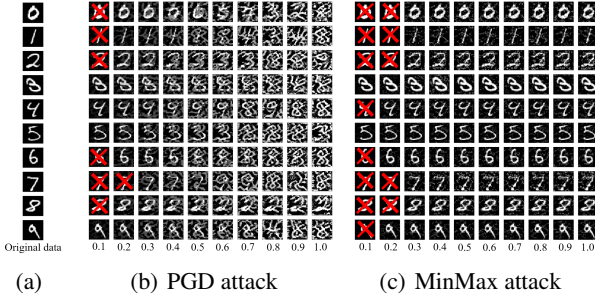


Figure 3: Comparison of untargeted supervised adversarial examples on MNIST. The unsuccessful adversarial examples are marked with red crosses. Each column corresponds to different ϵ values (L_∞ -norm perturbation bound) ranging from 0.1 to 1.0. Each row shows the adversarial examples of an original sample. MinMax attack using MINE yields adversarial examples with better visual quality than PGD attack, especially for large ϵ values.

Given the same ϵ value, MinMax attack yields adversarial examples with better visual quality. The results validate the importance of MINE as an effective similarity metric. In contrast, PGD attack aims to make full use of the L_∞ perturbation bound and attempts to modify every data dimension, giving rise to lower-quality adversarial examples. Similar results are observed for adversarially robust models (Madry et al. 2018; Zhang et al. 2019), as shown in SuppMat 6.16.

Moreover, the results also suggest that for MINE-based attacks, the L_∞ norm constraint on the perturbation is not critical for the resulting visual quality, which can be explained by the fact that MI is a fundamental information-theoretic similarity measure. When performing MINE-based attacks, we suggest not using the L_∞ norm constraint (by setting $\epsilon = 1$) so that the algorithm can fully leverage the power of MI to find a more diverse set of adversarial examples.

Next, we study three different unsupervised learning tasks. We only use the training samples and the associated training loss to generate UAEs. The post-hoc analysis reports the performance on the test data and the downstream classification accuracy. We report their improved adversarial robustness after data augmentation with MINE-UAEs in SuppMat 6.17.

4.4 UAE Improves Data Reconstruction

Data reconstruction using an autoencoder $\Phi(\cdot)$ that learns to encode and decode the raw data through latent representations is a standard unsupervised learning task. Here we use the default implementation of the following four autoen-

coders to generate UAEs based on the training data samples of MNIST and SVHN for data augmentation, retrain the model from scratch on the augmented dataset, and report the resulting reconstruction error on the original test set. The results of larger-scale datasets (CIFAR-10 and Tiny-ImageNet) are reported in SuppMat 6.11. All autoencoders use the L_2 reconstruction loss defined as $\|x - \Phi(x)\|_2$. We provide more details about the model retraining in SuppMat 6.10.

- **Dense Autoencoder (Cavallari, Ribeiro, and Ponti 2018):** The encoder and decoder have 1 dense layer separately and the latent dimension is 128/256 for MNIST/SVHN.
- **Sparse Autoencoder:** It has a sparsity enforcer (L_1 penalty on the training loss) that directs a network with a single hidden layer to learn the latent representations minimizing the error in reproducing the input while limiting the number of code words for reconstruction. We use the same architecture as Dense Autoencoder for MNIST and SVHN.
- **Convolutional Autoencoder¹:** The encoder uses convolution+relu+pooling layers. The decoder has reversed layer order with the pooling layer replaced by an upsampling layer.
- **Adversarial Autoencoder (Makhzani et al. 2016):** It is composed of an encoder, a decoder and a discriminator. The rationale is to force the distribution of the encoded values to be similar to the prior data distribution.

We also compare the performance of our proposed MINE-based UAE (MINE-UAE) with two baselines: (i) L_2 -UAE that replaces the objective of minimizing $I_\Theta(x, x + \delta)$ with maximizing the L_2 reconstruction loss $\|x - \Phi(x + \delta)\|_2$ in the MinMax attack algorithm while keeping the same attack success criterion; (ii) *Gaussian augmentation* (GA) that adds zero-mean Gaussian noise with a diagonal covariance matrix of the same constant σ^2 to the training data.

Table 4 shows the reconstruction loss and the ASR. The improvement of reconstruction error is measured with respect to the reconstruction loss of the original model (i.e., without data augmentation). We find that MINE-UAE can attain much higher ASR than L_2 -UAE and GA in most cases. More importantly, data augmentation using MINE-UAE achieves consistent and significant reconstruction performance improvement across all models and datasets (up to 56.7% on MNIST and up to 73.5% on SVHN), validating the effectiveness of MINE-UAE for data augmentation. On the other hand, in several cases L_2 -UAE and GA lead to notable performance degradation. The results suggest that MINE-UAE can be an effective plug-in data augmentation tool for boosting the performance of unsupervised machine learning models. Table 5 demonstrates UAEs can further improve data reconstruction when the original model already involves conventional augmented training data such as flip, rotation, and Gaussian noise. The augmentation setup is given in SuppMat 6.12. We also show the run time analysis of different augmentation method in SuppMat 6.7.

4.5 UAE Improves Representation Learning

The concrete autoencoder (Baln, Abid, and Zou 2019) is an unsupervised feature selection method which recognizes a subset of the most informative features through an additional

¹We use https://github.com/shibuiwilliam/Keras_Autoencoder

MNIST									
Autoencoder	Reconstruction Error (test set)					ASR (training set)			
	Original	MINE-UAE	L_2 -UAE	GA ($\sigma = 0.01$)	GA ($\sigma = 10^{-3}$)	MINE-UAE	L_2 -UAE	GA ($\sigma = 0.01$)	GA ($\sigma = 10^{-3}$)
Sparse	0.00561	0.00243 ($\uparrow 56.7\%$)	0.00348 ($\uparrow 38.0\%$)	0.00280 \pm 2.60e-05 ($\uparrow 50.1\%$)	0.00280 \pm 3.71e-05 ($\uparrow 50.1\%$)	100%	99.18%	54.10%	63.95%
Dense	0.00258	0.00228 ($\uparrow 11.6\%$)	0.00286 ($\downarrow 6.0\%$)	0.00244 \pm 0.00014 ($\uparrow 5.4\%$)	0.00238 \pm 0.00012 ($\uparrow 7.8\%$)	92.99%	99.94%	48.53%	58.47%
Convolutional	0.00294	0.00256 ($\uparrow 12.9\%$)	0.00364 ($\downarrow 23.8\%$)	0.00301 \pm 0.00011 ($\downarrow 2.4\%$)	0.00304 \pm 0.00015 ($\downarrow 3.4\%$)	99.86%	99.61%	68.71%	99.61%
Adversarial	0.04785	0.04581 ($\uparrow 4.3\%$)	0.06098 ($\downarrow 27.4\%$)	0.05793 \pm 0.00501 ($\downarrow 21\%$)	0.05544 \pm 0.00567 ($\downarrow 15.86\%$)	98.46%	43.54%	99.79%	99.83%
SVHN									
Sparse	0.00887	0.00235 ($\uparrow 73.5\%$)	0.00315 ($\uparrow 64.5\%$)	0.00301 \pm 0.00137 ($\uparrow 66.1\%$)	0.00293 \pm 0.00078 ($\uparrow 67.4\%$)	100%	72.16%	72.42%	79.92%
Dense	0.00659	0.00421 ($\uparrow 36.1\%$)	0.00550 ($\uparrow 16.5\%$)	0.00858 \pm 0.00232 ($\downarrow 30.2\%$)	0.00860 \pm 0.00190 ($\downarrow 30.5\%$)	99.99%	82.65%	92.3%	93.92%
Convolutional	0.00128	0.00095 ($\uparrow 25.8\%$)	0.00121 ($\uparrow 5.5\%$)	0.00098 \pm 3.77e-05 ($\uparrow 25.4\%$)	0.00104 \pm 7.41e-05 ($\uparrow 18.8\%$)	100%	56%	96.40%	99.24%
Adversarial	0.00173	0.00129 ($\uparrow 25.4\%$)	0.00181 ($\downarrow 27.4\%$)	0.00161 \pm 0.00061 ($\uparrow 6.9\%$)	0.00130 \pm 0.00037 ($\uparrow 24.9\%$)	94.82%	58.98%	97.31%	99.85%

Table 4: Comparison of data reconstruction by retraining the autoencoder on UAE-augmented data. The error is the average L_2 reconstruction loss of the test set. The improvement (in green/red) is relative to the original model. The attack success rate (ASR) is the fraction of augmented training data having smaller reconstruction loss than the original loss (see Table 1 for definition).

SVNH - Convolutional AE		
Augmentation	Aug. (test set)	Aug.+MINE-UAE (test set)
Flip + Rotation	0.00285	0.00107 ($\uparrow 62.46\%$)
Gaussian noise ($\sigma = 0.01$)	0.00107	0.00095 ($\uparrow 11.21\%$)
Flip + Rotation + Gaussian noise	0.00307	0.00099 ($\uparrow 67.75\%$)

Table 5: Performance of data reconstruction when retraining with MINE-UAE and additional augmented training data.

Dataset	Reconstruction Error (test set)		Accuracy (test set)		ASR
	Original	MINE-UAE	Original	MINE-UAE	MINE-UAE
MNIST	0.01170	0.01142 ($\uparrow 2.4\%$)	94.97%	95.41%	99.98%
Fashion MMIST	0.01307	0.01254 ($\uparrow 4.1\%$)	84.92%	85.24%	99.99%
Isotlet	0.01200	0.01159 ($\uparrow 3.4\%$)	81.98%	82.93%	100%
Coil-20	0.00693	0.01374 ($\downarrow 98.3\%$)	98.96%	96.88%	9.21%
Mice Protein	0.00651	0.00611 ($\uparrow 6.1\%$)	89.81%	91.2%	40.24%
Activity	0.00337	0.00300 ($\uparrow 11.0\%$)	83.38%	84.45%	96.52%

Table 6: Performance of representation learning by the concrete autoencoder and the resulting classification accuracy. The degradation on Coil-20 is explained in Section 4.5.

concrete select layer with M nodes in the encoder for data reconstruction. We apply MINE-UAE for data augmentation and use the same post-hoc classification evaluation procedure as in (Bain, Abid, and Zou 2019).

The six datasets and the resulting classification accuracy are reported in Table 6. We select $M = 50$ features for every dataset except for Mice Protein (we set $M = 10$) owing to its small data dimension. MINE-UAE can attain up to 11% improvement for data reconstruction and up to 1.39% increase in accuracy among 5 out of 6 datasets, corroborating the utility of MINE-UAE in representation learning and feature selection. The exception is Coil-20. A closer inspection shows that MINE-UAE has low ASR ($<10\%$) for Coil-20 and the training loss after data augmentation is significantly higher than the original training loss (see SuppMat 6.10). Therefore, we conclude that the degraded performance in Coil-20 after data augmentation is likely due to the limitation of feature selection protocol and the model learning capacity.

4.6 UAE Improves Contrastive Learning

The SimCLR algorithm (Chen et al. 2018) is a popular contrastive learning framework for visual representations. It uses

CIFAR-10			
Model	Loss (test set)	Accuracy (test set)	ASR
Original	0.29010	91.30%	-
MINE-UAE	0.26755 ($\uparrow 7.8\%$)	+1.58%	100%
CLAE (Ho and Vasconcelos 2020)	-	+0.05%	-

Table 7: Comparison of contrastive loss and the resulting accuracy on CIFAR-10 using SimCLR (Chen et al. 2018) (ResNet-18 with batch size = 512). The attack success rate (ASR) is the fraction of augmented training data having smaller contrastive loss than original loss. For CLAE (Ho and Vasconcelos 2020), we use the reported accuracy improvement (it shows negative gain in our implementation), though its base SimCLR model only has 83.27% test accuracy.

self-supervised data modifications to efficiently improve several downstream image classification tasks. We use the default implementation of SimCLR on CIFAR-10 and generate MINE-UAEs using the training data and the defined training loss for SimCLR. Table 7 shows the loss, ASR and the resulting classification accuracy by training a linear head on the learned representations. We find that using MINE-UAE for additional data augmentation and model retraining can yield 7.8% improvement in contrastive loss and 1.58% increase in classification accuracy. Comparing to (Ho and Vasconcelos 2020) using adversarial examples to improve SimCLR (named CLAE), the accuracy increase of MINE-UAE is 30x higher. Moreover, MINE-UAE data augmentation also significantly improves adversarial robustness (see SuppMat 6.17).

5 Conclusion

In this paper, we propose a novel framework for studying adversarial examples in unsupervised learning tasks, based on our developed per-sample mutual information neural estimator as an information-theoretic similarity measure. We also propose a new MinMax algorithm for efficient generation of MINE-based supervised and unsupervised adversarial examples and establish its convergence guarantees. As a novel application, we show that MINE-based UAEs can be used as a simple yet effective plug-in data augmentation tool and achieve significant performance gains in data reconstruction, representation learning, and contrastive learning.

Acknowledgments

This work was primarily done during Chia-Yi’s visit at IBM Research. Chia-Yi Hsu and Chia-Mu Yu were supported by MOST 110-2636-E-009-018, and we also thank National Center for High-performance Computing (NCHC) of National Applied Research Laboratories (NARLabs) in Taiwan for providing computational and storage resources.

References

- Athalye, A.; Carlini, N.; and Wagner, D. 2018. Obfuscated gradients give a false sense of security: Circumventing defenses to adversarial examples. *International Conference on International Conference on Machine Learning*.
- Balm, M. F.; Abid, A.; and Zou, J. 2019. Concrete autoencoders: Differentiable feature selection and reconstruction. In *International Conference on Machine Learning*, 444–453.
- Belghazi, M. I.; Baratin, A.; Rajeshwar, S.; Ozair, S.; Bengio, Y.; Courville, A.; and Hjelm, D. 2018. Mutual information neural estimation. In *International Conference on Machine Learning*, 531–540.
- Biggio, B.; and Roli, F. 2018. Wild patterns: Ten years after the rise of adversarial machine learning. *Pattern Recognition*, 84: 317–331.
- Bińkowski, M.; Sutherland, D. J.; Arbel, M.; and Gretton, A. 2018. Demystifying MMD GANs. In *International Conference on Learning Representations*.
- Brendel, W.; Rauber, J.; and Bethge, M. 2018. Decision-Based Adversarial Attacks: Reliable Attacks Against Black-Box Machine Learning Models. *International Conference on Learning Representations*.
- Candès, E. J.; and Wakin, M. B. 2008. An introduction to compressive sampling. *IEEE Signal Processing Magazine*, 25(2): 21–30.
- Carlini, N.; and Wagner, D. 2017a. Adversarial examples are not easily detected: Bypassing ten detection methods. In *ACM Workshop on Artificial Intelligence and Security*, 3–14.
- Carlini, N.; and Wagner, D. 2017b. Towards evaluating the robustness of neural networks. In *IEEE Symposium on Security and Privacy*, 39–57.
- Carmon, Y.; Ragunathan, A.; Schmidt, L.; Liang, P.; and Duchi, J. C. 2019. Unlabeled data improves adversarial robustness. *Neural Information Processing Systems*.
- Cavallari, G.; Ribeiro, L.; and Ponti, M. 2018. Unsupervised representation learning using convolutional and stacked autoencoders: a domain and cross-domain feature space analysis. In *IEEE SIBGRAPI Conference on Graphics, Patterns and Images (SIBGRAPI)*, 440–446.
- Cemgil, T.; Ghaisas, S.; Dvijotham, K. D.; and Kohli, P. 2020. Adversarially Robust Representations with Smooth Encoders. In *International Conference on Learning Representations*.
- Chen, P.-Y.; Zhang, H.; Sharma, Y.; Yi, J.; and Hsieh, C.-J. 2017. ZOO: Zeroth Order Optimization Based Black-box Attacks to Deep Neural Networks Without Training Substitute Models. In *ACM Workshop on Artificial Intelligence and Security*, 15–26.
- Chen, T.; Kornblith, S.; Norouzi, M.; and Hinton, G. 2018. A simple framework for contrastive learning of visual representations. In *International Conference on Machine Learning*.
- Donsker, M. D.; and Varadhan, S. S. 1983. Asymptotic evaluation of certain Markov process expectations for large time. IV. *Communications on Pure and Applied Mathematics*, 36(2): 183–212.
- Goodfellow, I. J.; Shlens, J.; and Szegedy, C. 2015. Explaining and harnessing adversarial examples. *International Conference on Learning Representations*.
- Heusel, M.; Ramsauer, H.; Unterthiner, T.; Nessler, B.; and Hochreiter, S. 2017. Gans trained by a two time-scale update rule converge to a local nash equilibrium. In *Advances in Neural Information Processing Systems*, 6626–6637.
- Hjelm, R. D.; Fedorov, A.; Lavoie-Marchildon, S.; Grewal, K.; Bachman, P.; Trischler, A.; and Bengio, Y. 2019. Learning deep representations by mutual information estimation and maximization. In *International Conference on Learning Representations*.
- Ho, C.-H.; and Vasconcelos, N. 2020. Contrastive learning with adversarial examples. In *Advances in Neural Information Processing Systems*.
- Liu, S.; Lu, S.; Chen, X.; Feng, Y.; Xu, K.; Al-Dujaili, A.; Hong, M.; and O’Reilly, U.-M. 2020. Min-max optimization without gradients: Convergence and applications to black-box evasion and poisoning attacks. In *International Conference on Machine Learning*.
- Lu, S.; Tsaknakis, I.; Hong, M.; and Chen, Y. 2020. Hybrid Block Successive Approximation for One-Sided Non-Convex Min-Max Problems: Algorithms and Applications. *IEEE Transactions on Signal Processing*, 68: 3676–3691.
- Madry, A.; Makelov, A.; Schmidt, L.; Tsipras, D.; and Vladu, A. 2018. Towards Deep Learning Models Resistant to Adversarial Attacks. *International Conference on Learning Representations*.
- Makhzani, A.; Shlens, J.; Jaitly, N.; Goodfellow, I.; and Frey, B. 2016. Adversarial autoencoders. *ICLR Workshop*.
- Miyato, T.; Maeda, S.-i.; Koyama, M.; and Ishii, S. 2018. Virtual adversarial training: a regularization method for supervised and semi-supervised learning. *IEEE transactions on pattern analysis and machine intelligence*, 41(8): 1979–1993.
- Nitin Bhagoji, A.; He, W.; Li, B.; and Song, D. 2018. Practical Black-box Attacks on Deep Neural Networks using Efficient Query Mechanisms. In *Proceedings of the European Conference on Computer Vision (ECCV)*, 154–169.
- Papernot, N.; McDaniel, P.; Goodfellow, I.; Jha, S.; Celik, Z. B.; and Swami, A. 2017. Practical black-box attacks against machine learning. In *ACM Asia Conference on Computer and Communications Security*, 506–519.
- Ranzato, M.; Huang, F. J.; Boureau, Y.-L.; and LeCun, Y. 2007. Unsupervised learning of invariant feature hierarchies with applications to object recognition. In *IEEE Conference on Computer Vision and Pattern Recognition*, 1–8.
- Razaviyayn, M.; Huang, T.; Lu, S.; Nouiehed, M.; Sanjabi, M.; and Hong, M. 2020. Nonconvex Min-Max Optimization: Applications, Challenges, and Recent Theoretical Advances. *IEEE Signal Processing Magazine*, 37(5): 55–66.

- Stanforth, R.; Fawzi, A.; Kohli, P.; et al. 2019. Are Labels Required for Improving Adversarial Robustness? *Neural Information Processing Systems*.
- Stutz, D.; Hein, M.; and Schiele, B. 2019. Disentangling adversarial robustness and generalization. In *Proceedings of the IEEE Conference on Computer Vision and Pattern Recognition*, 6976–6987.
- Su, D.; Zhang, H.; Chen, H.; Yi, J.; Chen, P.-Y.; and Gao, Y. 2018. Is robustness the cost of accuracy?—a comprehensive study on the robustness of 18 deep image classification models. In *Proceedings of the European Conference on Computer Vision (ECCV)*, 631–648.
- Szegedy, C.; Zaremba, W.; Sutskever, I.; Bruna, J.; Erhan, D.; Goodfellow, I.; and Fergus, R. 2013. Intriguing properties of neural networks. *arXiv preprint arXiv:1312.6199*.
- Tsipras, D.; Santurkar, S.; Engstrom, L.; Turner, A.; and Madry, A. 2019. Robustness may be at odds with accuracy. In *International Conference on Learning Representations*.
- Weng, T.-W.; Zhang, H.; Chen, P.-Y.; Yi, J.; Su, D.; Gao, Y.; Hsieh, C.-J.; and Daniel, L. 2018. Evaluating the Robustness of Neural Networks: An Extreme Value Theory Approach. *International Conference on Learning Representations*.
- Zhai, X.; Oliver, A.; Kolesnikov, A.; and Beyer, L. 2019. S4I: Self-supervised semi-supervised learning. In *Proceedings of the IEEE international Conference on Computer Vision*, 1476–1485.
- Zhang, H.; and Wang, J. 2019. Defense Against Adversarial Attacks Using Feature Scattering-based Adversarial Training. *Neural Information Processing Systems*.
- Zhang, H.; Yu, Y.; Jiao, J.; Xing, E.; El Ghaoui, L.; and Jordan, M. 2019. Theoretically principled trade-off between robustness and accuracy. In *International Conference on Machine Learning*, 7472–7482.
- Zhu, S.; Zhang, X.; and Evans, D. 2020. Learning Adversarially Robust Representations via Worst-Case Mutual Information Maximization. *International Conference on International Conference on Machine Learning*.
- Zhu, X.; and Goldberg, A. B. 2009. Introduction to semi-supervised learning. *Synthesis Lectures on Artificial Intelligence and Machine Learning*, 3(1): 1–130.

6 Supplementary Material

6.1 Codes

Our codes are provided as a zip file for review.

6.2 More Details on Per-sample MINE

Random Sampling We reshape an input data sample as a vector $x \in \mathbb{R}^d$ and independently generate K Gaussian random matrices $\{M_k\}_{k=1}^K$, where $M_k \in \mathbb{R}^{d' \times d}$. Each entry in M_k is an i.i.d zero-mean Gaussian random variable with standard deviation $1/d'$. The compressed samples $\{x_k\}_{k=1}^K$ of x is defined as $x_k = M_k x$. Similarly, the same random sampling procedure is used on $x + \delta$ to obtain its compressed samples $\{(x + \delta)_k\}_{k=1}^K$. In our implementation, we set $d' = 128$ and $K = 500$.

Convolution Layer Output Given a data sample x , we fetch its output of the 1st convolutional layer, denoted by $\text{conv}(x)$. The data dimension is $d' \times K$, where K is the number of filters (feature maps) and d' is the (flattend) dimension of the feature map. Each filter is regarded as a compressed sample denoted by $\text{conv}(x)_k$. Algorithm 2 summarizes the proposed approach, where the function T_θ is parameterized by a neural network θ based on the Donsker-Varadhan representation theorem (Donsker and Varadhan 1983), and T_I is the number of iterations for training the MI neural estimator $I(\theta)$.

Algorithm 2: Per-sample MINE via Convolution

- 1: **Require:** input sample x , perturbed sample $x + \delta$, 1st convolution layer output $\text{conv}(\cdot)$, MI neural estimator $I(\theta)$
 - 2: Initialize neural network parameters θ
 - 3: Get $\{\text{conv}(x)_k\}_{k=1}^K$ and $\{\text{conv}(x + \delta)_k\}_{k=1}^K$ via 1st convolution layer
 - 4: **for** t in T_I iterations **do**
 - 5: Take K samples from the joint distribution: $\{\text{conv}(x)_k, \text{conv}(x + \delta)_k\}_{k=1}^K$
 - 6: Shuffle K samples from $\text{conv}(x + \delta)$ marginal distribution: $\{\text{conv}(x + \delta)_{(k)}\}_{k=1}^K$
 - 7: Evaluate the mutual information estimate $I(\theta) \leftarrow \frac{1}{K} \sum_{k=1}^K T_\theta(\text{conv}(x)_k, \text{conv}(x + \delta)_k) - \log \left(\frac{1}{K} \sum_{k=1}^K \exp[T_\theta(\text{conv}(x)_k, \text{conv}(x + \delta)_{(k)})] \right)$
 - 8: $\theta \leftarrow \theta + \nabla_\theta I(\theta)$
 - 9: **Return** $I(\theta)$
-

6.3 Ablation Study of K for Random Sampling of Per-sample MINE

We follow the same setting as in Table 2 on CIFAR-10 and report the average persample-MINE, FID and KID results over 1000 samples when varying the value K in random sampling. The results in Table 8 show that both KID and FID scores decrease (meaning the generated adversarial examples are closer to the training data’s representations) as K increases, and they saturate when K is greater than 500. Similarly, the MI values become stable when K is greater than 500.

		CIFAR-10								
K		50	100	200	300	400	500	600	700	800
MI		1.35	1.53	1.86	2.05	2.13	2.32	2.33	2.35	2.38
FID		226.63	213.01	207.81	205.94	203.73	200.12	200.02	198.75	196.57
KID		14.7	12.20	10.8	10.02	9.59	8.78	8.81	8.22	8.29

Table 8: Comparison of MI, FID and KID when varying the value K in random sampling.

6.4 Additional Visual Comparisons

Visual Comparison of Supervised Adversarial Examples with $\epsilon = 0.03$ Similar to the setting in Figure 1, we compare the MINE-based supervised adversarial examples on CIFAR-10 with the L_∞ constraint $\epsilon = 0.03$ (instead of $\epsilon = 1$) in Figure 4.

Visual Comparison of Unsupervised Adversarial Examples Figure 5 shows the generated MINE-UAEs with $\epsilon = 1$ on SVHN using the convolutional autoencoder. We pick the 10 images such that their reconstruction loss is no greater than that of the original image, while they have the top-10 perturbation level measured by the L_2 norm on the perturbation $\|\delta^*\|_2$.

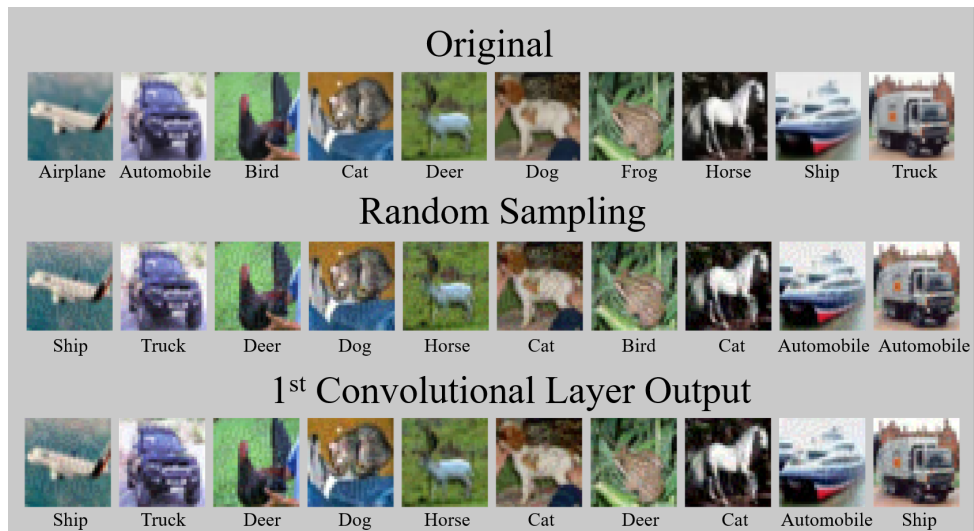


Figure 4: Visual comparison of MINE-based supervised adversarial examples (untargeted attack with $\epsilon = 0.03$) on CIFAR-10. Both random sampling and convolution output can be used to craft adversarial examples with high similarity. The label below each data sample indicates the predicted label, where the predicted label of the original image is the ground-truth label.

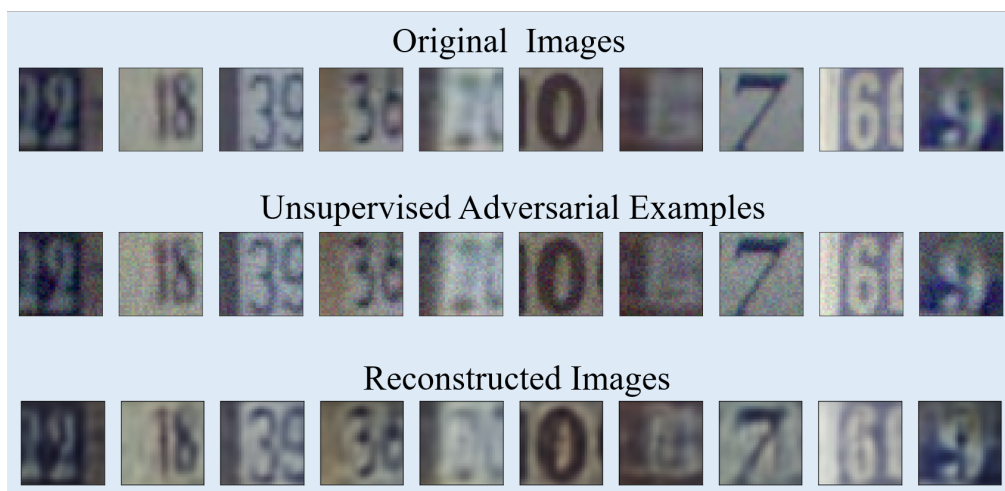


Figure 5: Visual comparison of MINE-based unsupervised adversarial examples on SVHN using convolutional autoencoder.

6.5 Binary Search for Penalty-based Attack Algorithm

Algorithm 3 summarizes the binary search strategy on the regularization coefficient c in the penalty-based methods. The search procedure follows the implementation in (Carlini and Wagner 2017b), which updates c per search step using a pair of pre-defined upper and lower bounds. The reported MI value of penalty-based method in Figure 2 is that of the current best search in c , where each search step takes 1000 iterations (i.e., $B = 9$ and $T' = 1000$).

Algorithm 3: Binary Search

```

1: Require: data sample  $x$ , attack criterion  $f_x(\cdot)$ , mutual information  $I_{\Theta}(x, x + \delta)$  and step sizes  $\alpha$ , perturbation bound  $\epsilon$ ,
   number of iterations  $T'$  in each search, total number of binary search steps  $B$ 
2: Initialization:  $lb = 10^{-3}$  (lower bound on  $c$ ),  $ub = 10^9$  (upper bound on  $c$ ),  $c = 10^{-3}$ ,  $I_{\Theta}^* = -\infty$ ,  $\delta^* = \text{null}$ 
3: for  $b$  in  $B$  binary search steps do
4:   for  $t$  in  $T'$  iterations do
5:      $\delta_{t+1} = \delta_t - \alpha \cdot (c \cdot \nabla f_x^+(x + \delta_t) - \nabla I_{\Theta}(x, x + \delta_t))$ 
6:     Project  $\delta_{t+1}$  to  $[\epsilon, -\epsilon]$  via clipping
7:     Project  $x + \delta_{t+1}$  to  $[0, 1]$  via clipping
8:     Compute  $I_{\Theta}(x, x + \delta_{t+1})$ 
9:     if  $f_x(x + \delta_{t+1}) \leq 0$  and  $I_{\Theta}(x, x + \delta_{t+1}) > I_{\Theta}^*$  then
10:       $\delta^* = \delta_{t+1}$ 
11:       $I_{\Theta}^* = I_{\Theta}(x, x + \delta_{t+1})$ 
12:     if  $f_x(x + \delta^*) \leq 0$  then
13:        $ub = \min\{ub, c\}$ 
14:       if  $ub < 10^9$  then
15:         Update  $c \leftarrow (lb + ub)/2$ 
16:       else
17:          $lb = \max\{lb, c\}$ 
18:         if  $ub < 10^9$  then
19:           Update  $c \leftarrow (lb + ub)/2$ 
20:         else
21:           Update  $c \leftarrow c \cdot 10$ 
22: Return  $\delta^*, I_{\Theta}^*$ 

```

6.6 Fixed-Iteration Analysis for Penalty-based Attack

To compare with the attack success of our MinMax Attack in Table 4, we fix $T=40$ total iterations for penalty-based attack. Specifically, for binary search with a times (each with b iterations), we ran $a \times b = 40$ total iterations with $(a,b)=(2,20)/(4,10)$ on convolutional autoencoder and MNIST. The attack success rate of $(2,20)/(4,10)/\text{MinMax(ours)}$ is $9.0/93.54/99.86\%$, demonstrating the effectiveness of our attack.

6.7 Run-time Analysis of Different Data Augmentation Methods

We perform additional run-time analysis for all methods using the same computing resources on the tasks in Tables 5 for MNIST and CIFAR-10. Table 9 shows the average run-time for generating one sample for each method. Note that although MINE-UAE consumes more time than others, its effectiveness in data augmentation is also the most prominent.

MNIST				
	MINE-UAE	L_2 -UAE	GA	Flip or Rotation
avg. per sample	0.059 sec.	0.025 sec.	0.012 sec.	9.18×10^{-5} sec.
CIFAR-10				
	MINE-UAE	L_2 -UAE	GA	Flip or Rotation
avg. per sample	1.735 sec.	0.37 sec.	0.029 sec.	0.00022 sec.

Table 9: Run-time analysis of different data augmentation methods.

6.8 Proof of Theorem 1

The proof incorporates the several special structures of this non-convex min-max problem, e.g., linear coupling between c and $f_x^+(x + \delta)$, the oracle of MINE, etc, which are not explored or considered adequately in prior arts. Therefore, the following theoretical analysis for the proposed algorithm is sufficiently different from the existing works on convergence analysis of min-max algorithms, although some steps/ideas of deviation are similar, e.g., descent lemma, perturbation term. For the purpose of the completeness, we provide the detailed proof as follows. To make the analysis more complete, we consider a slightly more general version of Algorithm 1, where in step 7 we use the update rule $c_{t+1} = (1 - \beta \cdot \gamma_t) \cdot c_t + \beta \cdot f_x^+(x + \delta_{t+1})$, where $\gamma_t \geq 0$ and $\gamma_t = 1/t^{1/4}$ is a special case used in Algorithm 1.

Proof: First, we quantify the descent of the objective value after performing one round update of δ and c . Note that the δ -subproblem of the attack formulation is

$$\delta_{t+1} = \arg \min_{\delta: x+\delta \in [0,1]^d, \delta \in [-\epsilon, \epsilon]^d} \langle c_t \nabla f_x^+(x + \delta_t) - I_{\Theta_t}(x, x + \delta_t), \delta - \delta_t \rangle + \frac{1}{2\alpha} \|\delta - \delta_t\|^2. \quad (1)$$

From the optimality condition of δ , we have

$$\langle \nabla c_t f_x^+(x + \delta_t) - \nabla I_{\Theta_t}(x, x + \delta_t) + \frac{1}{\alpha}(\delta_{t+1} - \delta_t), \delta_{t+1} - \delta_t \rangle \leq 0. \quad (2)$$

According to the gradient Lipschitz continuity of function $f_x^+(x)$ and $I_{\Theta}(x, x + \delta)$, it can be easily checked that $F(\delta, c)$ has gradient Lipschitz continuity with constant $L_f \bar{c} + L_I$. Then, we are able to have

$$c_t f_x^+(x + \delta_{t+1}) - I_{\Theta_t}(x, x + \delta_{t+1}) \quad (3)$$

$$\leq c_t f_x^+(x + \delta_t) - I_{\Theta_t}(x, x + \delta_t) + \langle c_t \nabla f_x^+(x + \delta_t) + \nabla I_{\Theta_t}(x, x + \delta_t), \delta_{t+1} - \delta_t \rangle + \frac{L_f \bar{c} + L_I}{2} \|\delta_{t+1} - \delta_t\|^2. \quad (4)$$

Substituting (2) into (4), we have

$$c_t f_x^+(x + \delta_{t+1}) - I_{\Theta_t}(x, x + \delta_{t+1}) \leq c_t f_x^+(x + \delta_t) - I_{\Theta_t}(x, x + \delta_t) - \left(\frac{1}{\alpha} - \frac{L_f \bar{c} + L_I}{2} \right) \|\delta_{t+1} - \delta_t\|^2. \quad (5)$$

From Assumption 2, we can further know that

$$c_t f_x^+(x + \delta_{t+1}) - I_{\Theta_{t+1}}(x, x + \delta_{t+1}) \leq c_t f_x^+(x + \delta_t) - I_{\Theta_t}(x, x + \delta_t) - \left(\frac{1}{\alpha} - \frac{L_f \bar{c} + L_I}{2} \right) \|\delta_{t+1} - \delta_t\|^2 + \eta. \quad (6)$$

When $\alpha_t \leq \frac{1}{L_f \bar{c} + L_I}$, we have

$$c_t f_x^+(x + \delta_{t+1}) - I_{\Theta_{t+1}}(x, x + \delta_{t+1}) \leq c_t f_x^+(x + \delta_t) - I_{\Theta_t}(x, x + \delta_t) - \frac{1}{2\alpha} \|\delta_{t+1} - \delta_t\|^2 + \eta. \quad (7)$$

Let function $f_x^{++}(c_t, \delta_t) = c_t f_x^+(x + \delta_t) - \mathbb{1}(c_t)$ and ξ_t denote the subgradient of $\mathbb{1}(c_t)$, where $\mathbb{1}(\cdot)$ denotes the indicator function. Since function $c f_x^+(x + \delta)$ is concave with respect to c , we have

$$\begin{aligned} & f_x^{++}(c_{t+1}, \delta_{t+1}) - f_x^{++}(c_t, \delta_{t+1}) \leq \langle f_x^+(x + \delta_{t+1}), c_{t+1} - c_t \rangle - \langle \xi_t, c_{t+1} - c_t \rangle \\ & = \langle f_x^+(x + \delta_{t+1}) - f_x^+(x, \delta_t), c_{t+1} - c_t \rangle + \langle f_x^+(x + \delta_t), c_{t+1} - c_t \rangle \\ & \quad - \langle \xi_{t+1}, c_{t+1} - c_t \rangle - \langle \xi_t - \xi_{t+1}, c_{t+1} - c_t \rangle \\ & \stackrel{(a)}{=} \frac{1}{\beta} (c_{t+1} - c_t)^2 + \gamma_t c_{t+1} (c_{t+1} - c_t) + (\xi_{t+1} - \xi_t) (c_{t+1} - c_t) \\ & \stackrel{(b)}{=} \frac{1}{\beta} (c_{t+1} - c_t)^2 + \gamma_{t-1} c_t (c_{t+1} - c_t) + (f_x^+(x + \delta_{t+1}) - f_x^+(x + \delta_t)) (c_{t+1} - c_t) \\ & \stackrel{(c)}{\leq} \frac{1}{2\beta} (c_t - c_{t-1})^2 + \frac{\beta l_f^2}{2} \|\delta_{t+1} - \delta_t\|^2 - \left(\frac{\gamma_{t-1}}{2} - \frac{1}{\beta} \right) (c_{t+1} - c_t)^2 \\ & \quad + \frac{\gamma_t}{2} c_{t+1}^2 - \frac{\gamma_{t-1}}{2} c_t^2 + \frac{\gamma_{t-1} - \gamma_t}{2} c_{t+1}^2 \end{aligned} \quad (8)$$

where in (a) we use the optimality condition of c -problem, i.e.,

$$\xi_{t+1} - f_x^+(x + \delta_{t+1}) + \frac{1}{\beta} (c_{t+1} - c_t) + \gamma_t c_{t+1} = 0, \quad (9)$$

and in (b) we substitute

$$\begin{aligned} \langle \xi_{t+1} - \xi_t, c_{t+1} - c_t \rangle &= \langle f_x^+(x + \delta_{t+1}) - f_x^+(x + \delta_t), c_{t+1} - c_t \rangle \\ &\quad - \frac{1}{\beta} \langle \underbrace{c_{t+1} - c_t - (c_t - c_{t-1})}_{:=v_t}, c_{t+1} - c_t \rangle - \langle \gamma_t c_{t+1} - \gamma_{t-1} c_t, c_{t+1} - c_t \rangle, \end{aligned} \quad (10)$$

and in (c) we use the quadrilateral identity and according to the Lipschitz continuity function $f_x^+(x + \delta)$, we have

$$(f_x^+(x + \delta_{t+1}) - f_x^+(x + \delta_t))(c_{t+1} - c_t) \leq \frac{\beta l_f^2}{2} \|\delta_{t+1} - \delta_t\|^2 + \frac{1}{2\beta} (c_{t+1} - c_t)^2, \quad (11)$$

and also

$$\begin{aligned} \gamma_{t-1} c_t (c_{t+1} - c_t) &= \frac{\gamma_{t-1}}{2} (c_{t+1}^2 - c_t^2 - (c_{t+1} - c_t)^2) \\ &= \frac{\gamma_t}{2} c_{t+1}^2 - \frac{\gamma_{t-1}}{2} c_t^2 - \frac{\gamma_{t-1}}{2} (c_{t+1} - c_t)^2 + \left(\frac{\gamma_{t-1} - \gamma_t}{2} \right) c_{t+1}^2. \end{aligned} \quad (12)$$

Combining (7) and (8), we have the descent of the objective function, i.e.,

$$\begin{aligned} c_{t+1} f_x^+(x + \delta_{t+1}) + I_{\Theta_{t+1}}(x, x + \delta_{t+1}) - (c_t f_x^+(x + \delta_t) + I_{\Theta_t}(x, x + \delta_t)) \\ \leq \frac{1}{2\beta} (c_t - c_{t-1})^2 - \left(\frac{1}{2\alpha} - \frac{\beta l_f^2}{2} \right) \|\delta_{t+1} - \delta_t\|^2 - \left(\frac{\gamma_{t-1}}{2} - \frac{1}{\beta} \right) (c_{t+1} - c_t)^2 \\ + \frac{\gamma_t}{2} c_{t+1}^2 - \frac{\gamma_{t-1}}{2} c_t^2 + \frac{\gamma_{t-1} - \gamma_t}{2} c_{t+1}^2 + \eta. \end{aligned} \quad (13)$$

Second, we need to obtain the recurrence of the size of the difference between two consecutive iterates. Note that the maximization problem is

$$c_{t+1} = \arg \max_{0 \leq c \leq \bar{c}} c f_x^+(x + \delta_{t+1}) - \frac{1}{2\beta} (c - c_t)^2 - \gamma_t c^2, \quad (14)$$

and the update of sequence $\{c_t\}$ can be implemented very efficiently as stated in the algorithm description as

$$c_{t+1} = P_{\mathcal{C}} \left((1 - \beta\gamma_t) c_t + \beta f_x^+(x + \delta_{t+1}) \right). \quad (15)$$

From the optimality condition of c -subproblem at the $t + 1$ th iteration, we have

$$-\langle f_x^+(x + \delta_{t+1}) - \frac{1}{\beta} (c_{t+1} - c_t) - \gamma_t c_{t+1}, c_{t+1} - c \rangle \leq 0, \forall c \in \mathcal{C} \quad (16)$$

also, from the optimality condition of c -subproblem at the t th iteration, we have

$$-\langle f_x^+(x + \delta_t) - \frac{1}{\beta} (c_t - c_{t-1}) - \gamma_{t-1} c_t, c - c_t \rangle \geq 0, \forall c \in \mathcal{C}. \quad (17)$$

Plugging in $c = c_t$ in (16), $c = c_{t+1}$ in (17) and combining them together, we can get

$$\frac{1}{\beta} v_{t+1} (c_{t+1} - c_t) + (\gamma_t c_{t+1} - \gamma_{t-1} c_t) (c_{t+1} - c_t) \leq (f_x^+(x + \delta_{t+1}) - f_x^+(x + \delta_t)) (c_{t+1} - c_t). \quad (18)$$

In the following, we will use this above inequality to analyze the recurrence of the size of the difference between two consecutive iterates. Note that

$$\begin{aligned} (\gamma_t c_{t+1} - \gamma_{t-1} c_t) (c_{t+1} - c_t) &= (\gamma_t c_{t+1} - \gamma_t c_t + \gamma_t c_t - \gamma_{t-1} c_t) (c_{t+1} - c_t) \\ &= \gamma_t (c_{t+1} - c_t)^2 + (\gamma_t - \gamma_{t-1}) c_t (c_{t+1} - c_t) \\ &= \gamma_t (c_{t+1} - c_t)^2 + \frac{\gamma_t - \gamma_{t-1}}{2} (c_{t+1}^2 - c_t^2 - (c_{t+1} - c_t)^2), \\ &= \frac{\gamma_t + \gamma_{t-1}}{2} (c_{t+1} - c_t)^2 - \frac{\gamma_{t-1} - \gamma_t}{2} (c_{t+1}^2 - c_t^2) \end{aligned} \quad (19)$$

and

$$v_{t+1} (c_{t+1} - c_t) = \frac{1}{2} \left((c_{t+1} - c_t)^2 + v_{t+1}^2 - (c_t - c_{t-1})^2 \right). \quad (20)$$

Substituting (19) and (20) into (18), we have

$$\begin{aligned} & \frac{1}{2\beta}(c_{t+1} - c_t)^2 - \frac{\gamma_{t-1} - \gamma_t}{2}c_{t+1}^2 \\ & \leq \frac{1}{2\beta}(c_t - c_{t-1})^2 - \frac{1}{2\beta}v_{t+1}^2 - \frac{\gamma_{t-1} - \gamma_t}{2}c_t^2 - \frac{\gamma_{t-1} + \gamma_t}{2}(c_{t+1} - c_t)^2 + (f_x^+(x + \delta_{t+1}) - f_x^+(x + \delta_t))(c_{t+1} - c_t) \end{aligned} \quad (21)$$

$$\stackrel{(a)}{\leq} \frac{1}{2\beta}(c_t - c_{t-1})^2 - \gamma_t(c_{t+1} - c_t)^2 - \frac{\gamma_{t-1} - \gamma_t}{2}c_t^2 + (f_x^+(x + \delta_{t+1}) - f_x^+(x + \delta_t))(c_{t+1} - c_t) \quad (22)$$

$$\stackrel{(b)}{\leq} \frac{1}{2\beta}(c_t - c_{t-1})^2 - \gamma_t(c_{t+1} - c_t)^2 - \frac{\gamma_{t-1} - \gamma_t}{2}c_t^2 + \frac{l_f^2}{2\gamma_t}\|\delta_{t+1} - \delta_t\|^2 + \frac{\gamma_t}{2}(c_{t+1} - c_t)^2 \quad (23)$$

$$\leq \frac{1}{2\beta}(c_t - c_{t-1})^2 - \frac{\gamma_t}{2}(c_{t+1} - c_t)^2 - \frac{\gamma_{t-1} - \gamma_t}{2}c_t^2 + \frac{l_f^2}{2\gamma_t}\|\delta_{t+1} - \delta_t\|^2 \quad (24)$$

where (a) is true because $0 < \gamma_t < \gamma_{t-1}$; in (b) we use Young's inequality.

Multiplying by 4 and dividing by $\beta\gamma_t$ on the both sides of the above equation, we can get

$$\begin{aligned} & \frac{2}{\beta^2\gamma_t}(c_{t+1} - c_t)^2 - \frac{2}{\beta}\left(\frac{\gamma_{t-1}}{\gamma_t} - 1\right)c_{t+1}^2 \\ & \leq \frac{2}{\beta^2\gamma_t}(c_t - c_{t-1})^2 - \frac{2}{\beta}\left(\frac{\gamma_{t-1}}{\gamma_t} - 1\right)c_t^2 - \frac{2}{\beta}(c_{t+1} - c_t)^2 + \frac{2l_f^2}{\beta\gamma_t^2}\|\delta_{t+1} - \delta_t\|^2 \end{aligned} \quad (25)$$

$$\begin{aligned} & \leq \frac{2}{\beta^2\gamma_{t-1}}(c_t - c_{t-1})^2 - \frac{2}{\beta}\left(\frac{\gamma_{t-2}}{\gamma_{t-1}} - 1\right)c_t^2 + \frac{2}{\beta}\left(\frac{1}{\gamma_t} - \frac{1}{\gamma_{t-1}}\right)(c_t - c_{t-1})^2 \\ & \quad + \frac{2}{\beta}\left(\frac{\gamma_{t-2}}{\gamma_{t-1}} - \frac{\gamma_{t-1}}{\gamma_t}\right)c_t^2 - \frac{2}{\beta}(c_{t+1} - c_t)^2 + \frac{2l_f^2}{\beta\gamma_t^2}\|\delta_{t+1} - \delta_t\|^2. \end{aligned} \quad (26)$$

Combining (13) and (26), we have

$$\begin{aligned} & c_{t+1}f_x^+(x + \delta_{t+1}) + I_{\Theta_{t+1}}(x, x + \delta_{t+1}) - \frac{\gamma_t}{2}c_{t+1}^2 + \frac{2}{\beta^2\gamma_t}(c_{t+1} - c_t)^2 - \frac{2}{\beta}\left(\frac{\gamma_{t-1}}{\gamma_t} - 1\right)c_{t+1}^2 \\ & \leq c_t f_x^+(x + \delta_t) + I_{\Theta_t}(x, x + \delta_t) - \frac{\gamma_{t-1}}{2}c_t^2 + \frac{2}{\beta^2\gamma_{t-1}}(c_t - c_{t-1})^2 - \frac{2}{\beta}\left(\frac{\gamma_{t-2}}{\gamma_{t-1}} - 1\right)c_t^2 \\ & \quad + \frac{1}{2\beta}(c_t - c_{t-1})^2 - \frac{1}{\beta}(c_{t+1} - c_t)^2 - \left(\frac{1}{2\alpha_t} - \left(\frac{\beta L_f^2}{2} + \frac{2L_f^2}{\beta\gamma_t^2}\right)\right)\|\delta_{t+1} - \delta_t\|^2 \\ & \quad + \frac{\gamma_{t-1} - \gamma_t}{2}c_{t+1}^2 + \frac{2}{\beta}\left(\frac{1}{\gamma_t} - \frac{1}{\gamma_{t-1}}\right)(c_t - c_{t-1})^2 + \frac{2}{\beta}\left(\frac{\gamma_{t-2}}{\gamma_{t-1}} - \frac{\gamma_{t-1}}{\gamma_t}\right)c_t^2 + \eta. \end{aligned} \quad (27)$$

Third, we construct the potential function to measure the descent achieved by the sequence. From (27), we have

$$\begin{aligned} \mathcal{P}_{t+1} & \leq \mathcal{P}_t - \frac{1}{2\beta}(c_{t+1} - c_t)^2 - \left(\frac{1}{2\alpha} - \left(\frac{\beta L_f^2}{2} + \frac{2L_f^2}{\beta\gamma_t^2}\right)\right)\|\delta_{t+1} - \delta_t\|^2 \\ & \quad + \frac{\gamma_{t-1} - \gamma_t}{2}c_{t+1}^2 + \frac{2}{\beta}\left(\frac{1}{\gamma_{t+1}} - \frac{1}{\gamma_t}\right)(c_{t+1} - c_t)^2 + \frac{2}{\beta}\left(\frac{\gamma_{t-2}}{\gamma_{t-1}} - \frac{\gamma_{t-1}}{\gamma_t}\right)c_t^2 + \eta \end{aligned} \quad (28)$$

where we define

$$\mathcal{P}_t := c_t f(x + \delta_t) + I_{\Theta_t}(x, x + \delta_t) + \left(\frac{1}{2\beta} + \frac{2}{\beta^2\gamma_{t-1}} + \frac{2}{\beta}\left(\frac{1}{\gamma_t} - \frac{1}{\gamma_{t-1}}\right)\right)(c_t - c_{t-1})^2 - \frac{\gamma_{t-1}}{2}c_t^2 - \frac{2}{\beta}\left(\frac{\gamma_{t-2}}{\gamma_{t-1}} - 1\right)c_t^2 \quad (29)$$

To have the descent of the potential function, it is obvious that we need to require

$$-\frac{1}{2\beta} + \frac{2}{\beta}\left(\frac{1}{\gamma_{t+1}} - \frac{1}{\gamma_t}\right) < 0, \quad (30)$$

which is equivalent to condition $1/\gamma_{t+1} - 1/\gamma_t \leq 0.25$ so that the sign in the front of term $(c_{t+1} - c_t)^2$ is negative.

When $1/\gamma_{t+1} - 1/\gamma_t \leq 0.2$, we have

$$\mathcal{P}_{t+1} \leq \mathcal{P}_t - \left(\frac{1}{2\alpha} - \left(\frac{\beta L_f^2}{2} + \frac{2L_f^2}{\beta\gamma_t^2}\right)\right)\|\delta_{t+1} - \delta_t\|^2 - \frac{1}{10\beta}(c_{t+1} - c_t)^2 + \frac{\gamma_{t-1} - \gamma_t}{2}c_{t+1}^2 + \frac{2}{\beta}\left(\frac{\gamma_{t-2}}{\gamma_{t-1}} - \frac{\gamma_{t-1}}{\gamma_t}\right)c_t^2 + \eta, \quad (31)$$

which can be also rewritten as

$$\left(\frac{1}{2\alpha} - \left(\frac{\beta l_f^2}{2} + \frac{2l_f^2}{\beta\gamma_t^2} \right) \right) \|\delta_{t+1} - \delta_t\|^2 + \frac{1}{10\beta} (c_{t+1} - c_t)^2 \leq \mathcal{P}_t - \mathcal{P}_{t+1} + \frac{\gamma_{t-1} - \gamma_t}{2} c_{t+1}^2 + \frac{2}{\beta} \left(\frac{\gamma_{t-2}}{\gamma_{t-1}} - \frac{\gamma_{t-1}}{\gamma_t} \right) c_t^2 + \eta. \quad (32)$$

Finally, we can provide the convergence rate of the MinMax algorithm as the following.

From the definition that

$$\mathcal{L}(\delta, c) := \begin{bmatrix} \delta - P_\Delta[\delta - \nabla_\delta F(\delta, c)] \\ c - P_C[c + \nabla_c F(\delta, c)] \end{bmatrix},$$

we know that

$$\begin{aligned} & \|\mathcal{L}(\delta_t, c_t)\| \\ & \leq \|\delta_{t+1} - \delta_t\| + \|\delta_{t+1} - P_\Delta(\delta_t - \nabla_\delta F(\delta_t, c_t))\| + |c_{t+1} - c_t| + |c_{t+1} - P_C(c_t + \nabla_c F(\delta_t, c_t))| \\ & \stackrel{(a)}{\leq} \|\delta_{t+1} - \delta_t\| + \left\| P_\Delta \left(\delta_{t+1} - (\nabla_\delta F(\delta_t, c_t) + \frac{1}{\alpha_t}(\delta_{t+1} - \delta_t)) \right) - P_\Delta(\delta_t - \nabla_\delta F(\delta_t, c_t)) \right\| \\ & \quad + |c_{t+1} - c_t| + \left| P_C \left(c_{t+1} + f(\delta_{t+1}) - \frac{1}{\beta}(c_{t+1} - c_t) - \gamma_t c_{t+1} \right) - P_C(c_t + f(\delta_t)) \right| \\ & \stackrel{(b)}{\leq} \left(2 + \frac{1}{\alpha} \right) \|\delta_{t+1} - \delta_t\| + \left(2 + \frac{1}{\beta} \right) |c_{t+1} - c_t| + \gamma_t c_{t+1} + |f(\delta_{t+1}) - f(\delta_t)| \\ & \stackrel{(c)}{\leq} \left(2 + \frac{1}{\alpha} + l_f \right) \|\delta_{t+1} - \delta_t\| + \left(2 + \frac{1}{\beta} \right) |c_{t+1} - c_t| + \gamma_t c_{t+1} \end{aligned} \quad (33)$$

where in (a) we use the optimality condition of subproblems; in (b) we use the triangle inequality and non-expansiveness of the projection operator; and (c) is true due to the Lipschitz continuity.

Then, we have

$$\|\mathcal{L}(\delta_t, c_t)\|^2 \leq 3 \left(2 + \frac{1}{\alpha} + l_f \right)^2 \|\delta_{t+1} - \delta_t\|^2 + 3 \left(2 + \frac{1}{\beta} \right)^2 (c_{t+1} - c_t)^2 + 3\gamma_t^2 \bar{c}^2. \quad (34)$$

When $\alpha \sim \gamma_t^2 \sim \eta \sim \mathcal{O}(1/\sqrt{T})$, and

$$\frac{1}{2\alpha} > \left(\frac{\beta l_f^2}{2} + \frac{2l_f^2}{\beta\gamma_t^2} \right), \quad (35)$$

then from (32) we can know that there exist constants C_1 and C_2 such that

$$C_1 \sqrt{T} \|\delta_{t+1} - \delta_t\|^2 + \frac{1}{10\beta} (c_{t+1} - c_t)^2 \leq \mathcal{P}_t - \mathcal{P}_{t+1} + \frac{\gamma_{t-1} - \gamma_t}{2} c_{t+1}^2 + \frac{2}{\beta} \left(\frac{\gamma_{t-2}}{\gamma_{t-1}} - \frac{\gamma_{t-1}}{\gamma_t} \right) \bar{c}^2 + \frac{C_2}{\sqrt{T}}, \quad (36)$$

and from (34) there exists constant C_3 such that

$$\|\mathcal{L}(\delta_t, c_t)\|^2 \leq C_3 T \|\delta_{t+1} - \delta_t\|^2 + 3 \left(2 + \frac{1}{\beta} \right)^2 (c_{t+1} - c_t)^2 + 3\gamma_t^2 \bar{c}^2 \quad (37)$$

Combining (36) and (37), we have

$$\begin{aligned} & \|\mathcal{L}(\delta_t, c_t)\|^2 \\ & \leq \max \left\{ \max\{C_1, C_3\} \sqrt{T}, \max \left\{ \frac{\sqrt{T}}{10\beta}, 3 \left(2 + \frac{1}{\beta} \right)^2 \right\} \right\} \left(\mathcal{P}_t - \mathcal{P}_{t+1} + \frac{\gamma_{t-1} - \gamma_t}{2} c_{t+1}^2 + \frac{2}{\beta} \left(\frac{\gamma_{t-2}}{\gamma_{t-1}} - \frac{\gamma_{t-1}}{\gamma_t} \right) \bar{c}^2 \right) \\ & \quad + 3\gamma_t^2 \bar{c}^2 + \frac{C_2}{\sqrt{T}}. \end{aligned} \quad (38)$$

Hence, there exist constant C_4 such that

$$\|\mathcal{L}(\delta_t, c_t)\|^2 \leq \sqrt{T} C_4 \left(\mathcal{P}_t - \mathcal{P}_{t+1} + \frac{\gamma_{t-1} - \gamma_t}{2} \bar{c}^2 + \frac{2}{\beta} \left(\frac{\gamma_{t-2}}{\gamma_{t-1}} - \frac{\gamma_{t-1}}{\gamma_t} \right) \bar{c}^2 \right) + 3\gamma_t^2 \bar{c}^2 + \frac{C_2}{\sqrt{T}}. \quad (39)$$

Applying the telescoping sum, we have

$$\frac{1}{T} \sum_{t=1}^T \|\mathcal{L}(\delta_t, c_t)\|^2 \leq \frac{C_4}{\sqrt{T}} \left((\mathcal{P}_1 - \mathcal{P}_{T+1}) + \frac{\gamma_0 \bar{c}^2}{2} + \frac{2\gamma_0 \bar{c}^2}{\gamma_1 \beta} \right) + 3\frac{\bar{c}^2}{\sqrt{T}} + \frac{C_2}{\sqrt{T}}. \quad (40)$$

According to the definition of $T(\varepsilon')$, we can conclude that there exists constant C such that

$$\|\mathcal{L}(\delta_{T(\varepsilon')}, c_{T(\varepsilon')})\|^2 \leq \frac{1}{T(\varepsilon')} \sum_{t=1}^{T(\varepsilon')} \|\mathcal{L}(\delta_t, c_t)\|^2 \leq \frac{C}{\sqrt{T(\varepsilon')}} \sim \mathcal{O}\left(\frac{1}{\sqrt{T(\varepsilon')}}\right), \quad (41)$$

which completes the proof. ■

6.9 More Discussion on UAEs and On-Manifold Adversarial Examples

Following (Stutz, Hein, and Schiele 2019), adversarial examples can be either on or off the data manifold, and only the on-manifold data samples are useful for model generalization. In the supervised setting, without the constraint on finding on-manifold examples, it is shown that simply using norm-bounded adversarial examples for adversarial training will hurt model generalization² (Stutz, Hein, and Schiele 2019).

As illustrated in Table 1, in the unsupervised setting we propose to use the training loss constraint to find on-manifold adversarial examples and show they can improve model performance.

6.10 More Details and Results on Data Augmentation and Model Retraining

The attack success rate (ASR) measures the effectiveness of finding UAEs. In Table 4, sparse autoencoder has low ASR due to feature selection, making attacks more difficult to succeed. MNIST’s ASR can be low because its low reconstruction loss limits the feasible space of UAEs.

Table 10 summarizes the training epochs and training loss of the models and datasets used in Section 4.4.

MNIST									
Autoencoder	Training Epochs				Reconstruction Error (training set)				
	Original	MINE-UAE	L_2 -UAE	GA ($\sigma = 10^{-2}/10^{-3}$)	Original	MINE-UAE	L_2 -UAE	GA ($\sigma = 10^{-2}$)	GA ($\sigma = 10^{-3}$)
Sparse	50	80	80	80	0.00563	0.00233	0.00345	0.00267±2.93e-05	0.00265±3.60e-5
Dense	20	30	30	30	0.00249	0.00218	0.00275	0.00231±0.00013	0.0023±0.00011
Convolutional	20	30	30	30	0.00301	0.00260	0.00371	0.00309±0.00013	0.00310±0.00015
Adversarial	50	80	80	80	0.044762	0.04612	0.06063	0.058711±0.00659	0.05551±0.00642
SVHN									
Sparse	50	80	80	80	0.00729	0.00221	0.00290	0.00283±0.00150	0.00275 ± 0.00081
Dense	30	50	50	50	0.00585	0.00419	0.00503	0.00781±0.00223	0.00781±0.00187
Convolutional	We set 100 epochs, but the training loss converges after 5 epochs				0.00140	0.00104	0.00131	0.00108±3.83e-05	0.00113±6.76e-05
Adversarial	We set 200 epochs and use the model with the lowest training loss				0.00169	0.00124	0.02729	0.00158±0.00059	0.00130±0.00036

Table 10: Details on the training epochs and losses for the datasets and models used in Section 4.4. The reconstruction error is the average L_2 reconstruction loss of the training set.

In Table 6, concrete autoencoder on Coil-20 has low ASR and the performance does not improve when using MINE-UAE for data augmentation. The original training loss is 0.00683 while the MINE-UAE training loss is increased to 0.01368. With careful parameter tuning, we were still unable to improve the MINE-UAE training loss. Therefore, we conclude that the degraded performance in Coil-20 after data augmentation is likely due to the imitation of feature selection protocol and the model learning capacity.

6.11 CIFAR-10 and Tiny-ImageNet Results

Table 11 shows the results using convolutional autoencoders on CIFAR-10 and Tiny-ImageNet using the same setup as in Table 4. Similar to the findings in Table 4 based on MNIST and SVHN, MINE-UAE attains the best loss compared to L_2 -UAE and GA.

CIFAR-10 (original loss: 0.00669) / Tiny-ImageNet (original loss: 0.00979)		
Reconstruction Error (test set) / ASR (training set)		
MINE-UAE	L_2 -UAE	GA ($\sigma = 10^{-3}$)
0.00562 (↑ 15.99%) / 99.98%	0.00613 (↑ 8.37%) / 89.84%	0.00564±1.31e-04 (↑ 15.70%) / 99.90%
0.00958 (↑ 21.45%) / 99.47%	0.00969 (↑ 1.02%) / 88.02%	0.00963±5.31e-05 (↑ 1.63%) / 99.83%

Table 11: Comparison of data reconstruction by retraining the convolutional autoencoder on UAE-augmented data using CIFAR-10 (first row) and Tiny-ImageNet (second row). The reconstruction error is the average L_2 reconstruction loss of the test set. The improvement (in green/red) is relative to the original model. The attack success rate (ASR) is the fraction of augmented training data having smaller reconstruction loss than the original loss (see Table 1 for definition).

²<https://davidstutz.de/on-manifold-adversarial-training-for-boosting-generalization>

6.12 More Details on Table 5

For all convolutional autoencoders, we use 100 epochs and early stopping if training loss converges at early stage. For data augmentation of the training data, we set the rotation angle = 10 and use both horizontal and vertical flip. For Gaussian noise, we use zero-mean and set $\sigma = 0.001$.

6.13 Hyperparameter Sensitivity Analysis

All of the aforementioned experiments were using $\beta = 0.1$ and $\alpha = 0.01$. Here we show the results on MNIST with convolution autoencoder (Section 4.4) and the concrete autoencoder (Section 4.5) using different combinations of α and β values. The results are comparable, suggesting that our MINE-based data augmentation is robust to a wide range of hyperparameter values.

MNIST							
		Convolution AE			Concrete AE		
$\alpha \backslash \beta$		0.05	0.1	0.5	0.05	0.1	0.5
0.01		0.00330	0.00256	0.00283	0.01126	0.01142	0.01134
0.05		0.00296	0.00278	0.00285	0.01129	0.01133	0.01138

Table 12: Comparison of reconstruction error (test set) of convolution and concrete autoencoders with different combinations of α and β values on MNIST.

6.14 Ablation Study on UAE’s Similarity Objective Function

As an ablation study to demonstrate the importance of using MINE for crafting UAEs, we replace the mutual information (MI) with L_2 -norm and cosine distance between $conv(x)$ and $conv(x + \delta)$ in our MinMAX attack algorithm. Table 13 compares the performance of retraining convolutional autoencoders with UAEs generated by the L_2 -norm, cosine distances and feature scattering-based proposed by Zhang and Wang (2019). It is observed that using MINE is more effective than these two distances.

MNIST (original reconstruction error: 0.00294)		
	Reconstruction Error (test set)	ASR (training set)
MINE-UAE	0.00256 ($\uparrow 12.9\%$)	99.86%
L_2 / cosine	0.002983 ($\downarrow 14.6\%$) / 0.002950 ($\downarrow 0.3\%$)	96.5% / 92%
Feature scattering-based	0.00268 ($\uparrow 8.9\%$)	99.96%
SVHN (original reconstruction error: 0.00128)		
MINE-UAE	0.00095 ($\uparrow 25.8\%$)	100%
L_2 / cosine	0.00096 ($\uparrow 18.75\%$) / 0.00100 ($\uparrow 21.88\%$)	94.52% / 96.79%
Feature scattering-based	0.001 ($\uparrow 21.6\%$)	99.76%

Table 13: Ablation Study on UAE’s similarity objective function using MinMax algorithm. The reconstruction error is the average L_2 reconstruction loss of the test set. The improvement (in green/red) is relative to the original model.

6.15 More Data Augmentation Runs

While the first run of UAE-based data augmentation is shown to improve model performance, here we explore the utility of more data augmentation runs. We conducted two data augmentation runs for sparse autoencoder on SVHN. We re-train the model with 1st-run UAEs, 2nd-run UAEs (generated by 1st-run augmented model) and original training data. The reconstruction error on the test set of 2nd data augmentation is 0.00199, which slightly improves the 1st-run result (0.00235). In general, we find that 1st-run UAE data augmentation has a much more significant performance gain comparing to the 1st-run results.

6.16 MINE-based Supervised Adversarial Examples for Adversarially Robust Models

Visual Comparison of Supervised Adversarial Examples for Adversarially Robust MNIST Models Figure 6 shows adversarial examples crafted by our attack against the released adversarially robust models trained using the Madry model (Madry et al. 2018) and TRADES (Zhang et al. 2019). Similar to the conclusion in Figure 3, our MINE-based attack can generate high-similarity and high-quality adversarial examples for large ϵ values, while PGD attack fail to do.

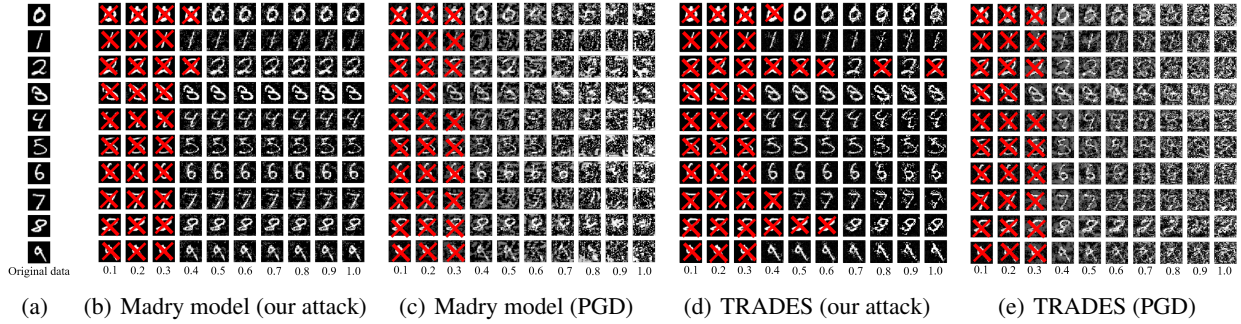


Figure 6: Visual comparison of untargeted supervised adversarial examples on two released adversarial robust MNIST models: Madry model (Madry et al. 2018) and TRADES (Zhang et al. 2019). We mark the unsuccessful adversarial examples with the red cross. Each row shows the crafted adversarial examples of an original sample. Each column corresponds to different ϵ values (L_∞ -norm perturbation bound) ranging from 0.1 to 1.0.

Attack Performance Figure 7 and 8 show the attack success rate (ASR) of released Madry and TRADES models against our attack and PGD attack on MNIST and CIFAR-10 with different L_∞ threshold ϵ . For all PGD attacks, we use 100 steps and set step size = $2.5 * \frac{\epsilon}{\text{number of steps}}$. For all our attacks against Madry model, we use learning rate = 0.01 and run 200 steps for MNIST, 100 steps for CIFAR-10. For all our attacks against TRADES model, we use learning rate = 0.01 and run 300 steps for MNIST, 200 steps for CIFAR-10. Both attacks have comparable attack performance. On MNIST, in the mid-range of the ϵ values, our attack ASR is observed to be lower than PGD, but it can generate higher-quality adversarial examples as shown in Figure 6.

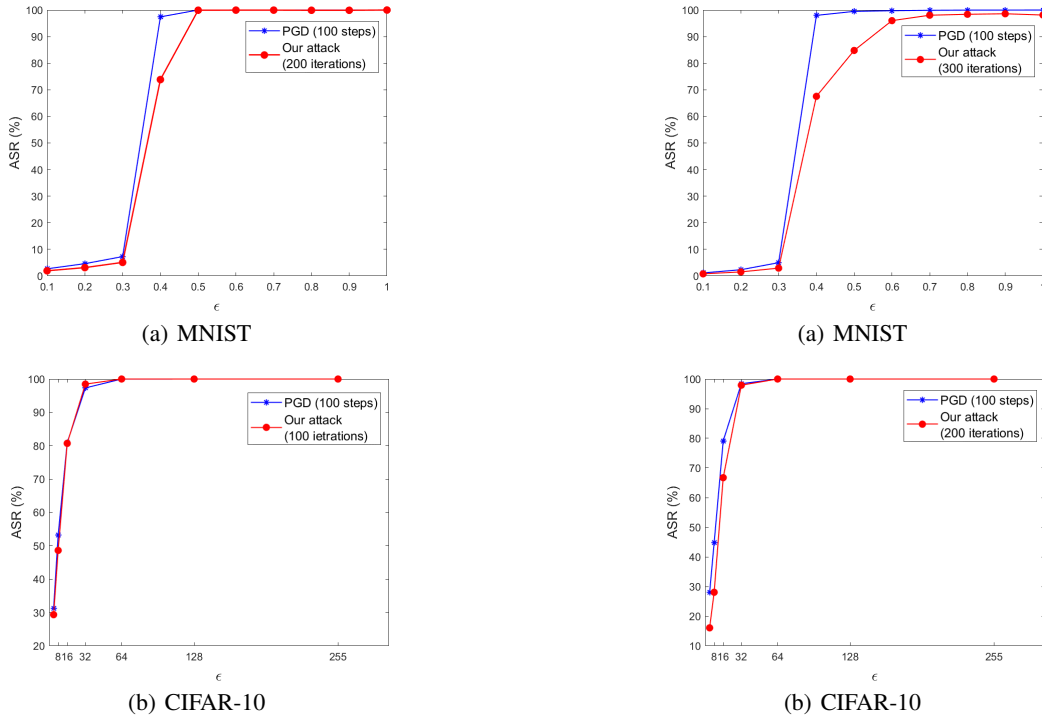


Figure 7: Attack success rate (ASR) of the released Madry models (Madry et al. 2018) on MNIST and CIFAR-10.

Figure 8: Attack success rate (ASR) of the released TRADES models on MNIST and CIFAR-10.

Adversarial Training with MINE-based Unsupervised Adversarial Examples We use the MNIST and CIFAR-10 models in Section 4.3 to compare the performances of standalone adversarial training (Adv. training) (Madry et al. 2018) and adversarial training plus data augmentation by MINE-based unsupervised adversarial examples (Adv. training-UAE) generated from convolutional Autoencoder. Figure 9 shows the attack success rate (ASR) of Adv. training model and Adv training-UAE against PGD attack. For all PGD attacks, we use 100 steps and set step size = $2.5 * \frac{\epsilon}{\text{number of steps}}$. When $\epsilon = 0.4$, Adv. training-UAE

model can still resist more than 60% of adversarial examples on MNIST. By contrast, ASR is 100% for Adv. training model. For CIFAR-10, ASR of Adv. training-UAE model is about 8% lower than Adv. training model when $\epsilon = 16$. We therefore conclude that data augmentation using UAE can improve adversarial training.

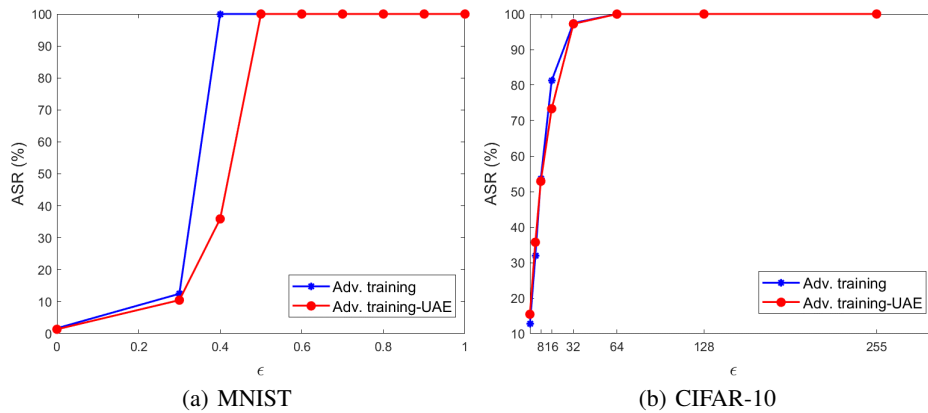


Figure 9: Performance evaluation of ASR for adv. training and adv. training-UAE against PGD attack with different ϵ value. Adv. training-UAE consistently shows lower or comparable ASR than adv. training, suggesting that data augmentation using UAE can improve adversarial training.

6.17 Improved Adversarial Robustness after Data Augmentation with MINE-UAEs

To evaluate the adversarial robustness after data augmentation with MINE-UAEs, we use the MNIST and CIFAR-10 models in Section 4.3 and Section 4.6, respectively. We randomly select 1000 classified correctly images (test set) to generate adversarial examples. For all PGD attacks, We set step size= 0.01 and use 100 steps.

In our first experiment (Figure 10 (a)), we train the convolutional classifier (Std) and Std with UAE (Std-UAE) generated from the convolutional autoencoder on MNIST. The attack success rate (ASR) of the Std-UAE is consistently lower than the Std for each ϵ value.

In the second experiment (Figure 10 (b)), the ASR of SimCLR-UAE is significantly lower than that of the original SimCLR model, especially for $\epsilon \leq 0.02$. When $\epsilon = 0.01$, SimCLR-UAE on CIFAR-10 can still resist more than 40% of adversarial examples, which is significantly better than the original SimCLR model. Based on the empirical results, we therefore conclude that data augmentation using UAE can improve adversarial robustness of unsupervised machine learning tasks.

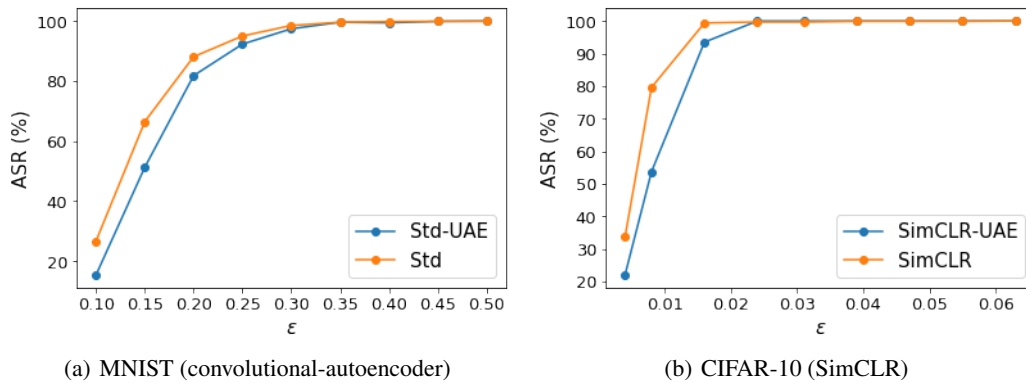


Figure 10: Robustness evaluation of attack success rate (ASR) for the original model (Std/SimCLR) and the models trained with UAE augmentation (Std-UAE/ SimCLR-UAE) against PGD attack with different ϵ values. Models trained with UAE shows better robustness (lower ASR) than original models, implying that data augmentation with UAE can strengthen the adversarial robustness.